SLAC-PUB-7376
December 1996

HOME PAGE

http://www.slac.stanford.edu/pubs/icfa/

ICFA INSTRUMENTATION BULLETIN*

The publication of the ICFA Instrumentation Bulletin is an activity of the Panel on Future Innovation and Development of ICFA (International Committee for Future Accelerators).

• Fall 1996 Issue

* Supported by the Department of Energy contract DE-AC03-76SF00515.

ICFA INSTRUMENTATION BULLETIN

The publication of the ICFA Instrumentation Bulletin is an activity of the Panel on Future Innovation and Development of ICFA (International Committee for Future Accelerators). The Bulletin reports on research and progress in the field of instrumentation with emphasis on application in the field of high-energy physics. It encourages issues of generic instrumentation.

Publisher : Stanford Linear Accelerator Center
SLAC Publications Department
Stanford, CA 94309, U.S.A.

Editor : J. Va'vra

Web Technical Advisers : J. Schwiening and T. Pavel

http://www.slac.stanford.edu/pubs/icfa/

Cover: The illustration depicts L. J. Waghenaer's marine atlas, "The Mariner's Mirror," published in 1588. Lucas Janszoon Waghenaer was born in Holland in the 1530s. He became a famous ship pilot in his time. In 1584, he published the atlas ("Spieghel der Zeevaerdt") which was greatly valued among mariners for centuries. This was not due only to the map content, but also to the detailed knowledge of navigation techniques of that time. The atlas, as it appears on our page, is the same one used for the Dutch to English translation.

1996-1997 Conference List

- Frontier Detectors for Frontier Physics
  7th Pisa Meeting on Advanced Detector
  25-31 May 1997, La Biodola, Isola d'Elba (Italy).

- IEEE Real Time 1997 Conference
  22-26 September 1997, Beaune, France

- VII ICFA School on Instrumentation in Elementary Particle Physics
  July 7-19, 1997, Leon, Guanajuato, Mexico
  e-mail: gherrera@fis.cinvestav.mx

Table of Contents

3-DIMENSIONAL SIMULATION OF ELECTRON AVALANCHES IN LOW PRESSURE WIRE CHAMBERS AND PROPORTIONAL COUNTERS

H. Průchová *
GSF - Forschungszentrum fur Umwelt und Gesundheit
Institut fur Strahlenschutz, Neuherberg
85758 Oberschleissheim, Germany
on leave from Czech Technical University, Prague, Czech Republic

and

B. Franěk
Rutherford Appleton Laboratory, Chilton, Didcot, Oxon, OX11 0QX,
United Kingdom

ABSTRACT

Monte Carlo code AVALAN was designed to simulate an electron avalanche development under any operating conditions of a proportional counter such as different gas pressures and electric fields. It alows to study any temporal and space aspects of the avalanche development. Initial simulations were performed for low pressure cylindrical counter filled with methane gas. Some results from these simulations are discussed.

1 Introduction

The design of proportional counters and wire chambers intended for various applications could be significantly facilitated by a better understanding of the electron motion in a force field (electric and/or magnetic) in various gases and their mixtures. This is especially true in the case of counters operating at low gas pressures and high electric fields such as, for example, counters used in

*partially supported by *Commission of European Community* (contract FI3P-CT920045)

microdosimetry. The region close to the anode in these counters is characterized by extremely high values of E/N (E being the electric field strength and N the number of gas molecules per unit volume). In such regions, moving electrons find themselves in the so called 'non-equilibrium state' and the traditional methods used for describing the motion of electron swarms in an electric field, and based mainly on the solution of the Boltzman equation, are not applicable.

There were attempts to improve these traditional methods and to take the non-equilibrium effects into account but only with limited success and invoking additional and rather unclear assumptions. See, for example, Segur et al [1], [2], [3]. Also, in recent years, several methods have been published based on microscopical Monte Carlo modeling of electron motion in gases [4], [5], [6], [7], [8]. However, these latter methods either address only few macroscopic aspects of the electron avalanche development such as the gas gain (e.g. [4], [5]) or make approximations which are only valid at small values of E/N ([6], [7], [8]). For example they do not take the magnitude and the gradient of the electric field into account when calculating the time step and base it only on the mean free path.

We have developed a Monte Carlo technique suitable for the simulation of electron motion and electron avalanche development in counters operating under any operating conditions. This alows the study of any aspect (temporal and spatial) of these processes in any level of detail.

2 Method

The Monte Carlo program, AVALAN, was developed to simulate the electron motion in a force field and all electron interactions with gas molecules. The program starts with a given number of initial electrons deposited at chosen space points at time t=0. These electrons are then 'simultaneously' followed in the force field of the counter in given small time steps dts. In every time interval $(t, t + dts)$, each individual electron existing at time t is followed from time t to time $t + dts$ in the following way:

The electron is followed in small and variable length time intervals t_{elm} which are fractions of dts. Before every step, the magnitude of t_{elm} is calculated from the magnitude of the velocity of the electron and from the magnitude of the force field and its gradient. The necessary requirement in this calculation is that t_{elm} must be sufficiently small in order that the relative change of the vector of the electron's velocity during this time is very small. Also, it is required that the vector of the force field at the new electron's position differs only very little from that at its original position (before t_{elm}). Satisfying these requirements means, that in the time interval t_{elm} the trajectory of the electron can be approximated by a straight line with constant velocity and the force field can be considered constant. Before every step t_{elm}, the program also decides by random number generation whether the electron will interact with a gas molecule before reaching the end of t_{elm}.

For this purpose the tables of measured total cross-sections for electron-molecule processes for a given gas (gases) are used. If it turns out that the electron will interact before reaching the end of t_{elm}, the time t_{elm} is shortened so that the electron will interact exactly at the time $t + t_{elm}$. The electron is then 'moved' in time t_{elm} and its new vector of position and velocity are calculated. If the electron interacts at the end of the time interval t_{elm}, then first the type of the interaction is randomly chosen using the relative values of measured cross-sections for various electron-molecule processes and then the interaction is simulated resulting in a change of the electron's velocity vector. The following interactions were taken into consideration: elastic, excitation (rotational excitation, vibrational excitation and neutral dissociation) and ionization. At the present time, mainly due to the lack of reliable data in the given energy range, angular distributions in all these interactions are approximated by isotropic distribution. In nonelastic collisions the electron also loses energy and this is taken into account using available data. In ionization collisions a new electron is created and it shares the energy remaining after the collision with the original electron. This secondary electron is also isotropically scattered.
When the electron finally reaches the time $t + dts$, then all the new electrons created in the time interval $(t, t+dts)$ in the ionization collisions and which are descendants of this electron, are followed in the same way until they all reach the time $t + dts$.

At the end of every time step, dts, the positions and velocities of all the electrons existing at time $t + dts$ are recorded. Simulation ends when all electrons are captured by the anode (anodes) of the detector. Fig. 1 shows the simulated trajectory of one of the electrons in an avalanche projected onto the plane perpendicular to the anode wire (the little circle at the origin). The dots show the positions at which the positive ions were created during the avalanche process. The picture demonstrates the level of detail of the simulation.

3 Preliminary results

Initial simulations have been performed for a half inch cylindrical proportional counter used in microdosimetry (so called TEPC) with a cathode diameter of 1.27 cm and an anode diameter of $7\mu m$. The counter was assumed to be filled with pure methane. The latest available cross-section data for this gas were collected and used [9]-[19]. Simulations of the avalanche development have been performed at various gas pressures between 6.9 and 69 torr and the same anode voltage of $760V$. The coordinate system of the counter has been chosen such that the anode wire is perpendicular to the x, y plane and goes through the origin. In all simulations we started with a single electron released far from the anode wire at $(x = 4000\mu m, y = 0, z = 0)$. Fig. 2 and 3 show a typical avalanche development in this counter. We have scanned many such pictures to determine the important features and also to find out how to quantitatively describe the avalanche so that

we could then study the avalanche development statistically (using samples of many independent avalanches). Based on this scanning, we have introduced a number of so called *avalanche parameters* which we then use for this purpose. Examples of these parameters are gain, radial or time extent of an avalanche *etc.* Due to the lack of space we cannot discuss these statistical studies here but will merely point out some of the more noteworthy results:

At these pressures, the electron avalanche completely surrounds the anode wire (see Figs. 2 and 3). This is a very different situation from the *conventional* counters (operating usually at 1atm) where the avalanche is developing and contained on the side of the anode wire from which the primary electron is approaching. This effect increases with decreasing gas pressure and is caused by the fact that, as the mean free path between the collisions with gas molecules becomes comparable to the diameter of the anode, an electron has more chance to miss the wire and cause ionizations on the other side of the wire. This effect can be quite clearly seen on Fig. 1.

Also, the avalanche is not 'homogeneous' but consists of many *partial* avalanches started by what we call *seeding* electrons in the *seeding region*. The seeding region provides an explanation for the nature of the dependence of certain avalanche parameters on gas pressure. The existence of the seeding region can be clearly seen from Fig. 4. In this figure the points are the x coordinates of all electrons existing at a given time. Fig. 5 shows a similar picture of the same avalanche zooming only on one of the partial avalanches. The squares are space-time points where the positive ions were created. Rotation of the electrons around the anode wire is quite clearly apparent. These two figures also demonstrate how various time characteristics of the avalanche development can be studied.

4 Conclusion

The Monte Carlo code has been developed to simulate the motion of electrons in a force field of a proportional counter and electron's interactions with gas molecules. The method does not make any assumptions about the operating conditions of a counter and works reliably in the most extreme situations such as at high E/N. The only uncertainties come from the measured experimental data on electron-molecule interactions. It enables to study all aspects of spacial and temporal development of the electron avalanche in proportional counters and wire chambers and should help in their design.

References

[1] Segur, P., Peres, I., Boeuf, J.P., Bordage, M.C. Microscopic Calculation of the Gas Gain in Cylindrical Proportional Counters. Rad. Prot. Dosimetry Vol. 29, No 1/2, 23 (1989)

[2] Segur, P., Colautti, P., Moutarde, C., Conte, V., Alkaa,A., Talpo, G., Tornielli, Rabehi, A. Comparison between Experimental and Theoretical Determination of the Space Variation of the Gas Gain inside Low Pressure TEPC's. Radiation Protection Dosimetry Vol. 52, Nos 1-4, pp. 65-71 (1994)

[3] P. Segur, L. Peres, J.P. Boeuf and J. Barthe, *Radiation Protection Dosimetry* **31** (1990) 107–118

[4] Cukier, M., Dhez, P., Jaegle, P. Etude Experimentale et Theorique de l'Amplification Gazeuse dans un Compteur Proportional Cylindrique a Basse Pression. Rev. Phys. Appl. 7, pp. 357 - 365 (1972)

[5] Matoba, M., Hirose, T., Sakae, T., Kametani, H., Ijiri, H., Shintake, T. Three Dimensional Monte Carlo Simulation of the Electron Avalanche around an Anode Wire of a Proportional Counter. IEEE Transaction on Nuclear Science, Vol. NS-32, No. 1, 541 (1985)

[6] Groh, J. Computersimilation der Elektronenlawine in zylindersymmetrischen elektrischen Feldern. Dissertation Universitat Hamburg (1989)

[7] Groh, J., Schenuit, E., Spitzer, H. Computer Simulation of the Electron Avalanche in Cylindrically Symmetric Fields. NIM A**283**, 730 (1989)

[8] Groh, J., Schenuit, E., Spitzer, H. Computer Simulation of the Electron Avalanches in Argon-Methane filled Wire Chambers. NIM A**293**, 537 (1990)

[9] B. Schmidt, Anisotropic low energy electron collision cross sections for methane derived from transport coefficients. *J.Phys.B: Mol. Opt. Phys.* **24** (1991) 4809–4820. and private communication.

[10] B.Lohmann and S.J.Buckman, Low-energy electron scattering from methane. *J.Phys.B: Mol. Opt. Phys.* **19** (1986) 2565–2570.

[11] H. Tanaka and L. Boesten, Elastic DCS for $e + CH_4$ collisions, $1.5 - 100eV$ *J.Phys.B: Mol. Opt. Phys.* **24** (1991) 821–832.

[12] T. Sakae, S. Sumiyoshi, E. Murakami, Y. Matsumoto, K. Ishibashi and A. Katase, Scattering of electrons by CH_4, CF_4 and SF_6 in the $75 - 700eV$ range. *J.Phys.B: Mol. Opt. Phys.* **22** (1989) 1385–1394.

[13] B. Mapstone and W.R. Newell, Vibrational excitation of methane by electron impact *J.Phys.B: Mol. Opt. Phys.* **27** (1994) 5761–5772.

[14] H. Chatham, D. Hills, R. Robertson and A. Gallagher, *J.Chem.Phys.* **81** (1984) 1770.

[15] H.F. Winters, *J.Chem.Phys.* **63** (1975) 3462.

[16] S.F. Biagi, A Multiterm Boltzmann Analysis of Drift Velocity, Diffusion, Gain and Magnetic-field Effects in Argon-Methane-Water-Vapour Mixtures. *Nucl.Instr. and Methods A* **283** (1989) 716–722; and private communication

[17] H. Nishimura and H. Tawara, Total electron impact ionisation cross sections for simple hydrocarbon molecules. *J.Phys.B: At.Mol.Phys.* **27** (1994) 2063–2074.

[18] D. Rapp and P. Englander-Golden, Total Cross Sections for Ionization and Attachment in Gases by Electron Impact. I. Positive Ionisation. *J.Chem.Phys.* **43**(5) (1965) 1464–1479.

[19] O. J. Orient, S. K. Srivastava, Electron impact ionisation of H_2O, CO, CO_2 and CH_4. *J.Phys.B: At.Mol.Phys.* **20** (1987) 3923–3936.

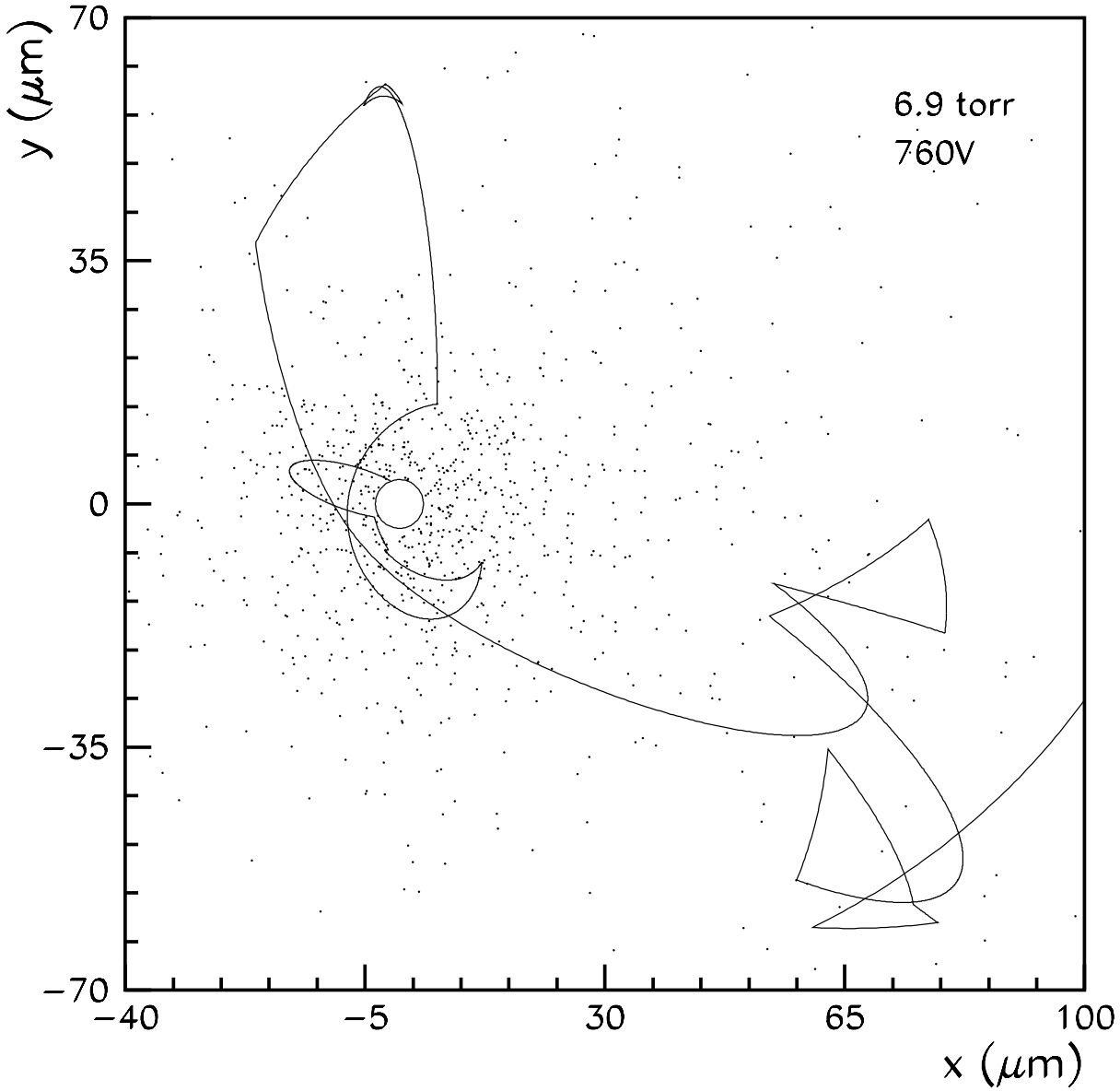

Figure 1: Simulated trajectory of one of the electrons in an avalanche projected onto the plane perpendicular to the anode wire (the little circle at the origin). The dots show the positions at which the positive ions were created during the avalanche process.

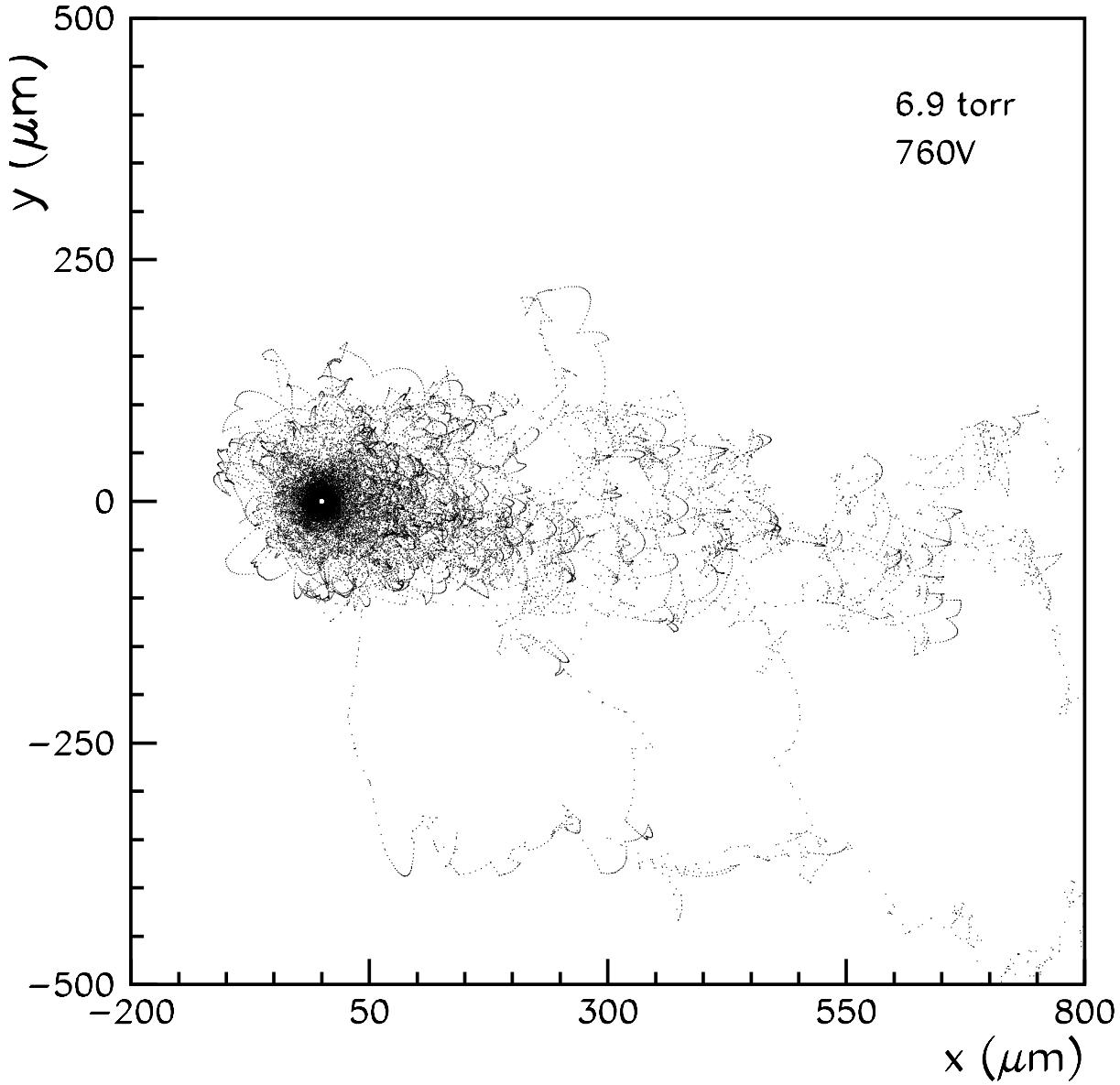

Figure 2: Trajectories of all the electrons in a typical avalanche projected into xy plane. Not all the trajectory points are shown.

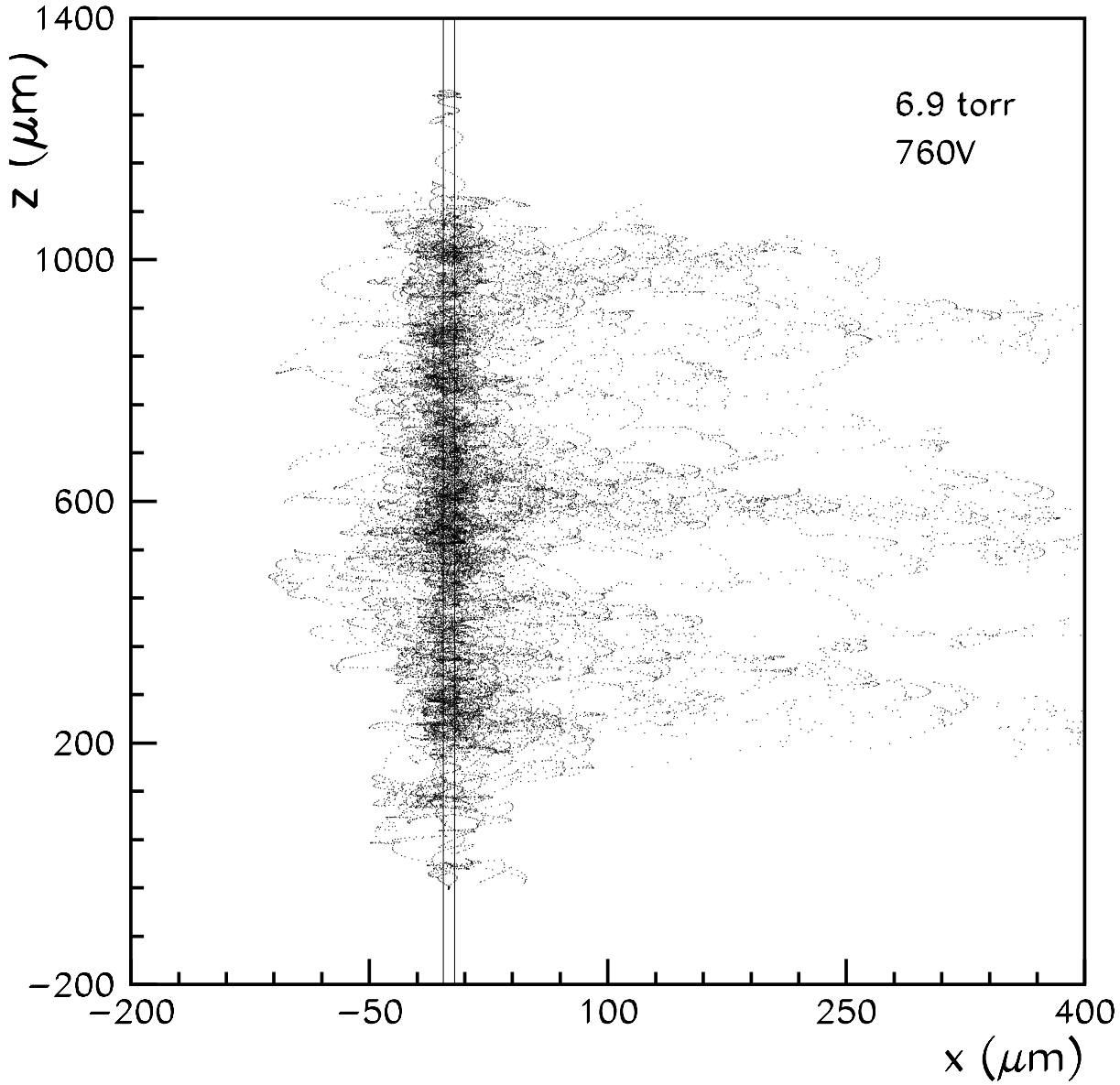

Figure 3: Trajectories of all the electrons in a typical avalanche projected into xz plane. Not all the trajectory points are shown.

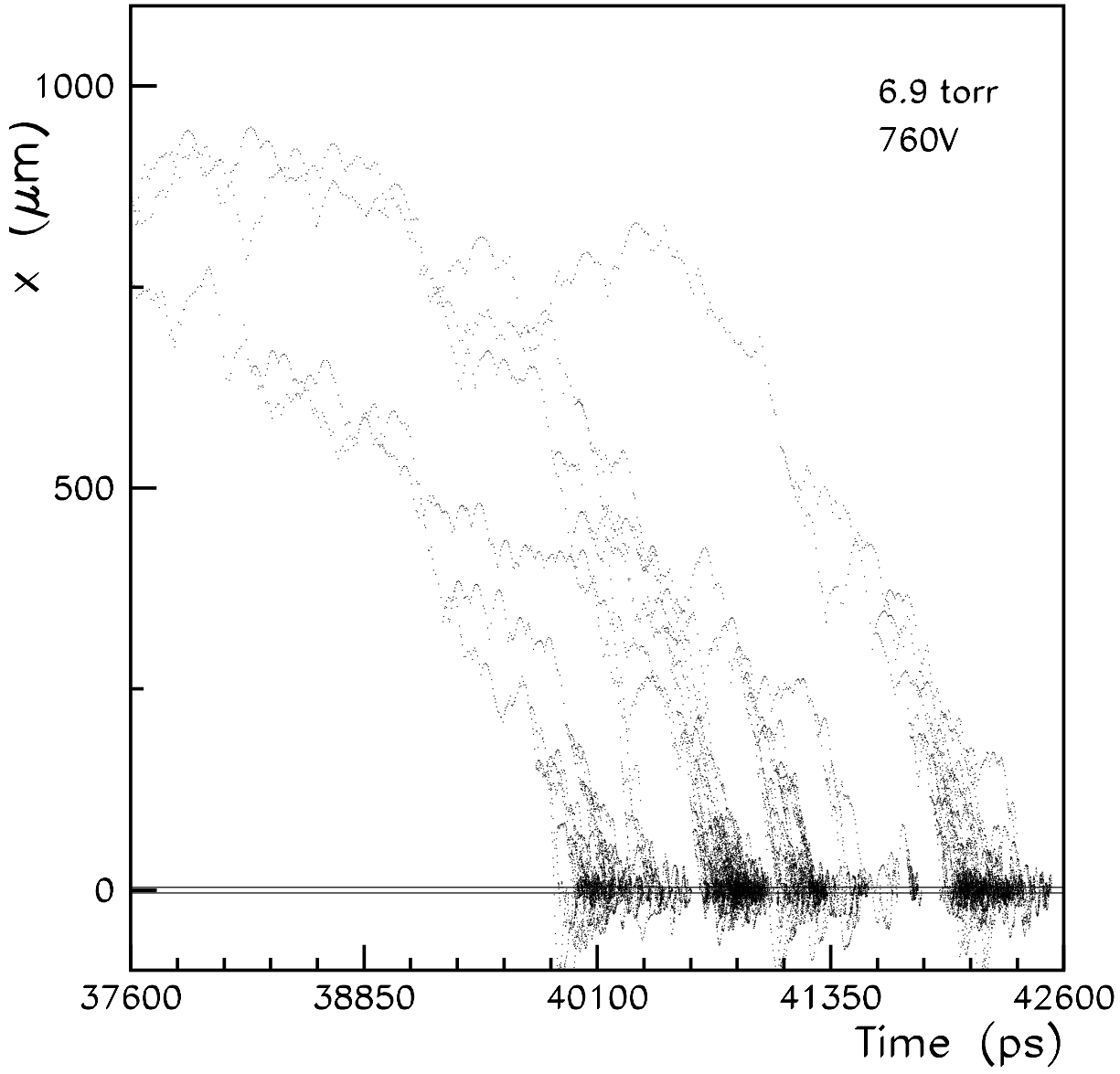

Figure 4: The space-time picture of a typical avalanche development. The points are the x coordinates (vertical axis) of all electrons existing at a given time (horizontal axis).

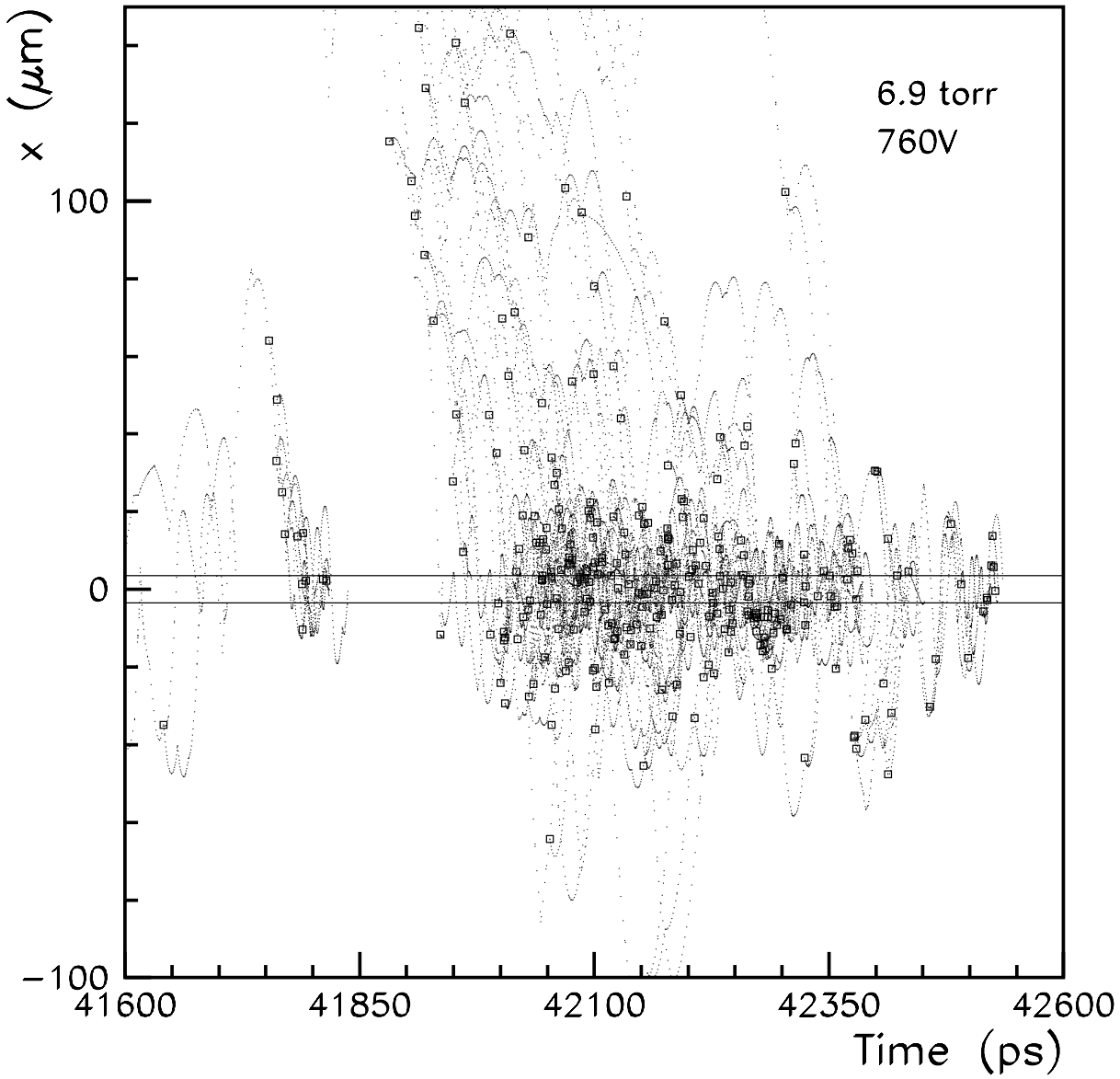

Figure 5: The space-time picture of avalanche development. Same as Fig. 4 but zooming on one of the *partial avalanches*. The little squares are the space-time points where the positive ions were created

CERAMIC ELECTRON MULTIPLIER

G. Comby

CEA/DSM/DAPNIA - CE Saclay
91191 Gif-sur-Yvette - France
Tel : (1) 6908 2229, Fax : (1) 6908 3024
E-mail: comby@hep.cea.fr

Abstract

The **C**eramic **E**lectron **M**ultipliers (CEM) is a compact, robust, linear and fast multi-channel electron multiplier. The **M**ulti **L**ayer **C**eramic **T**echnique (MLCT) allows to build metallic dynodes inside a compact ceramic block. The activation of the metallic dynodes enhances their **s**econdary **e**lectron **e**mission (SEE). The CEM can be used in multi-channel photomultipliers, multi-channel light intensifiers, ion detection, spectroscopy, analysis of time of flight events, particle detection or Cherenkov imaging detectors.

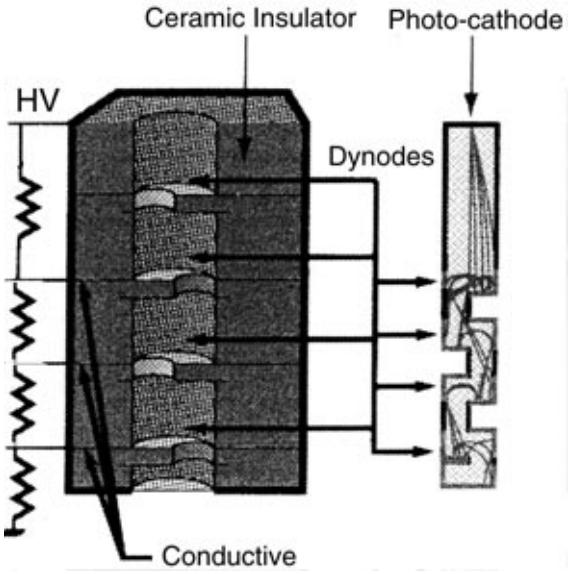

Fig. 1 - A principle of the CEM

CEM operating principle

The CEM operation principle is the same as a classical PM tube. A voltage divider establishes a voltage between metallic cavities. The metallic walls of the cavities are activated to enhance their secondary electron emission (SEE), which changes them to dynodes. Amplification of the dynode structure, coupled with a good electron transfer efficiency, creates a large amplification factor. Our dynode structure design inhibits the ion feed-back, which could damage a photocathode surface. The structure does not need the vacuum glass or metal envelope, or socket feed-through and allows to build very compact sensors.

CEM CHARACTERISTICS

Mechanical aspect

RAw ceramic sheets 0.05 to 0.5 mm thick are punched (to form cavities), painted with a conductive ink (to make conductive walls and conductive strips, in order to connect all inner elements to the external pads), packaged and fired to get a compact ceramic block. After that, the cavity walls are metalized by the chemical electro-plating technique to form metallic dynodes. The ceramic design enables a resistance to shocks and vibrations.

The CEM can be sized to a particular application. Up to 20 to 30 ceramic sheets can be packaged to build sophisticated structures. The standard dimensions of the MLCT components goes from 10 to 60 mm^2. Larger sizes, up to 200 mm^2, can be achieved, if necessary. CEM are produced by a High Technology mass production Industry. Such production allows uniformity, reproducibility, low cost of the components. After the metal coating of the cavities and the operating tests, these components are delivered ready-to-use by the ceramist.

Vacuum & Chemical aspect

The alumina and metals, together with a high firing temperature (~1500°C), produce very clean ceramic surfaces suitable for ultra high vacuum technique. In addition, a chemical stability of alumina preserves the physical properties in an alkali atmosphere.

Dynode electrical insulation

The resistivity of a 0.25 mm thick inter-dynode-stage is larger than 200 GΩ at 200 Volts, allowing a very stable operation. A dynode surface activation with cesium does not affect this stability.

Dynode activation

The dynode activation is achieved by a chemical process involving alkali metals plated on the electrode, and cesium vapor, creating a very thin and reactive layer with low work function. The secondary emission can be enhanced by a factor 10 to 20 depending on the nature of the elements and the preparation of the metallic surfaces. Several ways exist so that: each manufacturer proceeds with its own technique to produce efficient emitting dynodes. In our study, a SbCs layer was formed on the dynodes-cavities from electro-plated antimony. We achieved a dynode gain of 6-7 per stage voltage of 200 Volts. We obtained a total gain of ~1.5×10^3 using six stages. A very stable operation was observed. A larger number of the dynodes can produce a multiplication factor up to ~10^6.

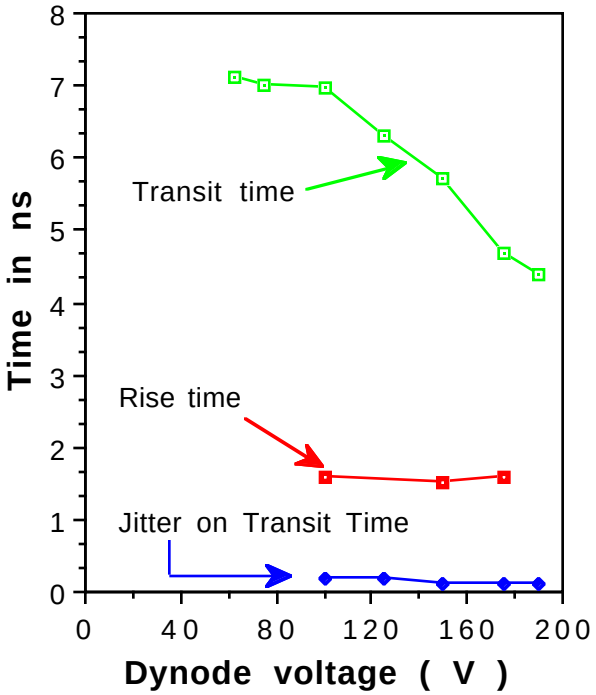

Fig. 2 - Dependence of a transit time, rise time and a jitter on the dynode voltage.

Dynamic characteristics

We measured a rise time of 1.6 ns for a dynode voltage of a 180 Volts, using a laser flashes with a 900 ps duration. When the dynode voltage increased from 60 to 200 Volts, the transit time decreased from 7 to 4.5 ns, and the corresponding jitter decreased from 150 to 100 ps.

No modification of the electron multiplication was observed during the double-pulse tests when the delay between flashes decreased to zero. The absence of a recovery time proves that a continuous pixel sensitivity and a gain independent of the flash delay.

Linearity

No saturation affects were detected in the output pulses, up to a charge of 250 pC at a dynode voltage of 180 V .

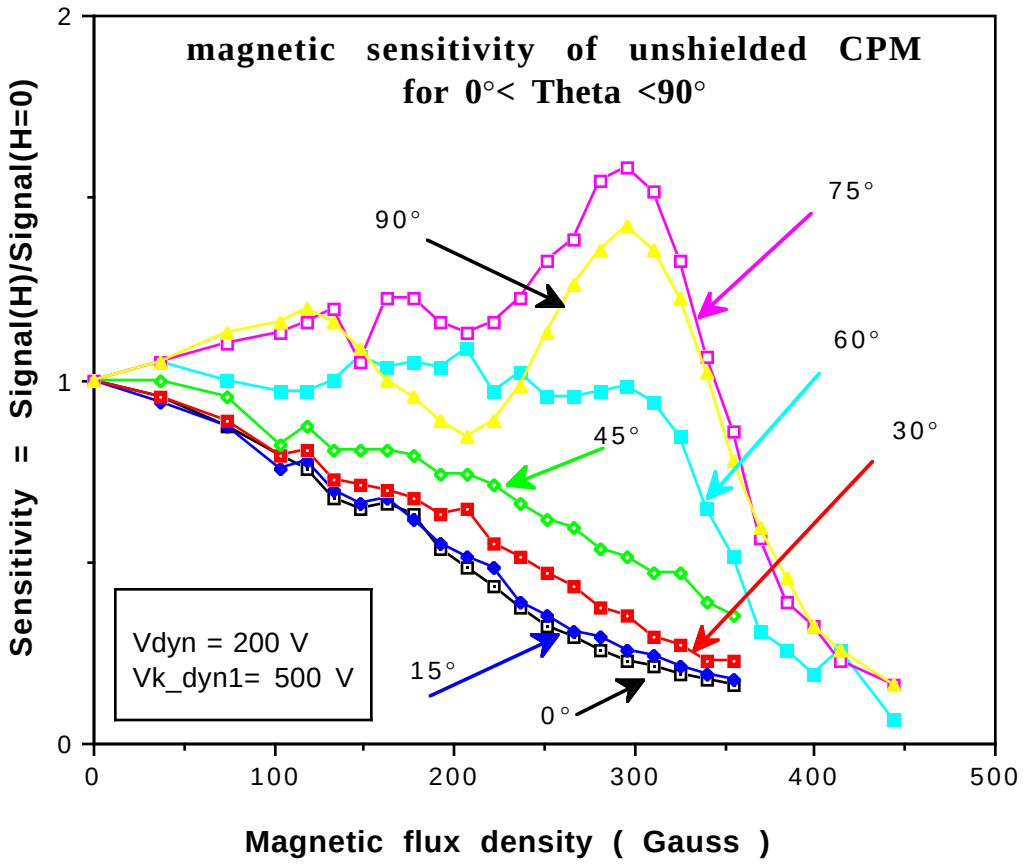

Fig.3 Sensitivity of the CEM output on the magnetic field.

Operation in magnetic field

The small dimension of the cavities and their compact structure enables to work in a magnetic field up to 200 Gauss for CEM channel axis parallel to field H, and up to 360 Gauss when perpendicular to field. A symmetrical arrangement of the dynodes preserves the CEM output signal whatever is a Phi rotation around the Anode/Cathode axis from 0 to 360°.

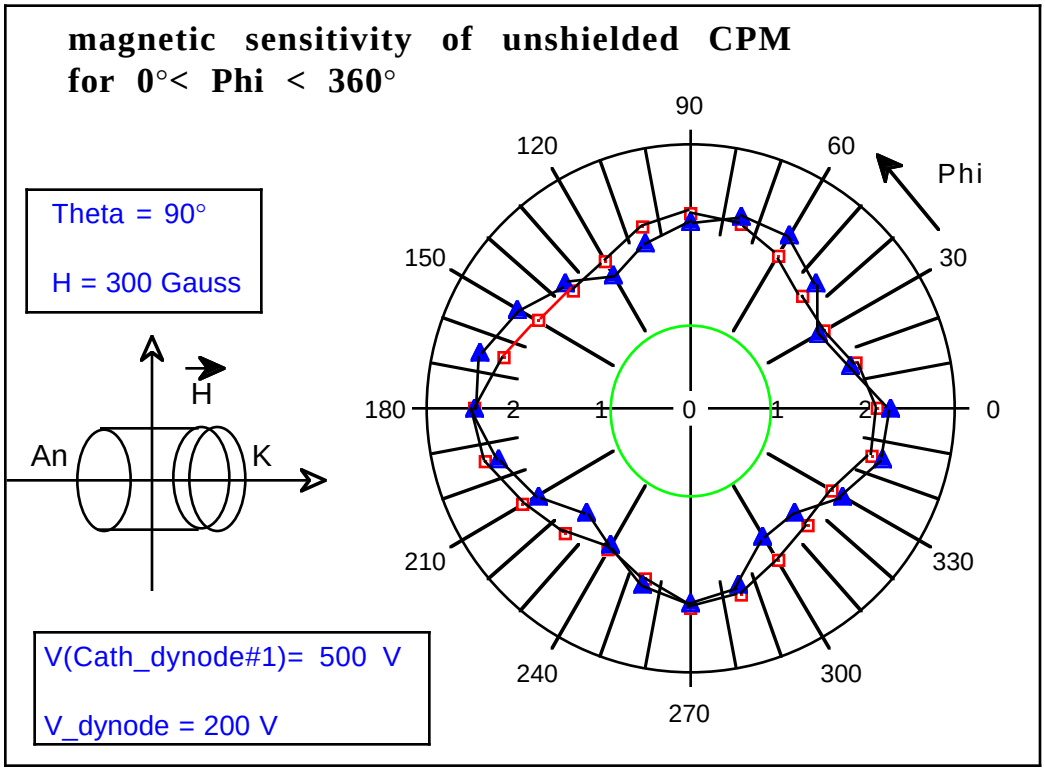

Fig.4 Sensitivity of the CEM output on the magnetic field.

CEM Applications

The manufacture of sealed detectors (assembling, activation, sealing) necessitates the use of the transfer method in order to preserve the high quality of the activation.

The CEMs included in open setups require a special dynode coating to assume convenient secondary electron emission level and to tolerate the break-down of the vacuum.

Equiping the CEM with a glass window bearing the photocathode and a ceramic socket including the output pixel pads, produces compact multi-pixel ceramic photomultiplier.

Replacing in a previous application, the output socket by a glass bearing phosphorescent pads, produces a multi-pixel light intensifier.

Included in the detection group of a mass spectrometer, the CEM allows to make a dynamic imagery of the ion detection.

CEM can be also adapted:

- to build ultra high vacuum sensors
- to enhance the electronic flux of pulsed photocathode injectors
- to form multi-lens electrostatic structure to guide and to distribute electron flux

REFERENCES

(1) G. Comby and F. Lehar, - A ceramic multi-channel electron multiplier for a new multi-channel PM-, presented at the Int. Workshop on Heavy Scintillators for Scientific and Industrial Applications, Chamonix, 1992.

(2) G. Comby, F. Lehar, E. Chassaing, G. Lorthioir, - Status of the ceramic multichannel PM tube -, Nucl. Instr. and Meth. A 343 (1994) 263-267.

(3) G. Comby, M. Karolak, Y. Piret, J.P. Mouly et al, Performances of multi-channel ceramic photomultiplier -, Int. conference on Inorganic Scintillators and their Applications, DELFT University of Technology, the Netherlands, 1995.

THE PRESAMPLER FOR THE FORWARD AND REAR CALORIMETER IN THE ZEUS DETECTOR

A.Bamberger[4], A.Bornheim[1], J.Crittenden[1], H.-J.Grabosch[3], M.Grothe[1], L.Hervas[7], E.Hilger[1], U.Holm[5], D.Horstmann[5], V.Kaufmann[4], A.Kharchilava[3], U.Kötz[2], D.Kummerow[5], U.Mallik[6], A.Meyer[3], M.Nowoczyn[5], R.Ossowski[1], S.Schlenstedt[3], H.Tiecke[8], W.Verkerke[8], J.Vossebeld[8], M.Vreeswijk[8], S.M.Wang[6], J.Wu[6]

[1] Physikalisches Institut der Universität Bonn, Bonn, Germany
[2] Deutsches Elektronen-Synchrotron DESY, Hamburg, Germany
[3] DESY-IfH Zeuthen, Zeuthen, Germany
[4] Fakultät für Physik der Universität Freiburg i.Br., Freiburg i.Br., Germany
[5] Hamburg University, II. Institute of Exp. Physics, Hamburg, Germany
[6] University of Iowa Physics and Astronomy Dept, Iowa City, USA
[7] Univer. Autonoma Madrid, Depto de Fisica Teorica, Madrid, Spain
[8] NIKHEF and University of Amsterdam, Netherlands

ABSTRACT

The ZEUS detector at HERA has been supplemented with a presampler detector in front of the forward and rear calorimeters. It consists of a segmented scintillator array read out with wavelength-shifting fibers. We discuss its design, construction and performance. Test beam data obtained with a prototype presampler and the ZEUS prototype calorimeter demonstrate the main function of this detector, i.e. the correction for the energy lost by an electron interacting in inactive material in front of the calorimeter.

1 Introduction

The material situated between the electron-proton interaction point and the front face of the uranium-scintillator calorimeter within the ZEUS detector at HERA [1] leads to a degradation of the calorimetric energy measurement of the particles produced in the interaction. We have constructed a presampler detector, now installed directly in front of the forward and rear ZEUS calorimeter sections, with the goal of measuring this energy degradation on an event–by–event basis. The detector consists of a layer of scintillator tiles; wavelength-shifting fibers, embedded in the scintillator, guide the scintillation light to photomultipliers. Particles which shower in the material in front of the presampler lead to an increased particle multiplicity which is measured by the presampler. The combined information from the presampler and the calorimeter allows an event-by-event measurement of the energy loss in front of the calorimeter and thus allows to recover the energy scale and energy resolution of the ZEUS calorimeter. We describe the production and performance of the optical components, the assembly of the presampler detector, the readout system and the calibration system. We summarize results on the response of the individual tiles to cosmic rays and results of a test of a prototype presampler in combination with the ZEUS calorimeter prototype in a CERN test beam.

2 Scintillator/fiber combination

The segmentation of the presampler matches that of the ZEUS calorimeter [2] hadronic sections, 20 x 20 cm^2. The scintillation light is read out by wavelength-shifting fibers embedded in the scintillator and transported by clear fibers to a photomultiplier. Since the calibration of the presampler is performed with minimum–ionising particles (MIP) we require a photoelectron yield of at least 5 photoelectrons per MIP at the photocathode of the photomultiplier (PMT).

We have investigated several combinations of scintillator material, fiber material and fiber layout to optimize light yield and response uniformity, resulting in the following choice:

- scintillator material SCSN38 (Kuraray Co. Ltd), 5 mm thick with dimension 203 x 198.5 mm^2; tiles are cut and diamond-polished. Six grooves, parallel to the long edge, are machined in the tiles with an ordinary saw blade *; the grooves are 1.2 mm wide, 1.5 mm deep and equally spaced over the surface.
- six fibers read out one tile; they are glued † in the grooves in the scintillator.

*The blade has a diameter of 95 mm and is 1.2 mm thick; the revolution speed was 2000-2500 turns/min and progressed with about 10cm/min; as coolant we used a mixture of water and detergent.

†NE 581 Optical Cement with hardener

- WLS fiber material Y11 (Kuraray Co. Ltd) double clad, 1 mm diameter, 23 cm long with a sputtered Al mirror at one end.
- a 1 mm diameter double clad transparent polystyrene fiber DCLG (Kuraray Co. Ltd) guides the light to the photomultiplier; the fiber is 3 m long and is glued to the WLS fiber.
- wrapping of the tile in Tyvek paper (quality Q173-D, DuPont) paper.

2.1 Fiber production.

The faces of the fibers were smoothed in steps with sandpaper of various granularities down to a grain size of a few microns. For this purpose a mounting support was designed which held 50 fibers individually. In this manner the cladding was prevented from cracking and the resulting face was perpendicular to the fibre-axis. One face of each WLS-fiber was also polished and then aluminized by vacuum evaporation in order to prevent light loss through this end.
For an optimal joint between the WLS-fiber and the clear readout-fiber a gluing procedure was chosen [‡]. Steel tubes, with an inner (outer) diameter of 1.1 (1.2) mm, served for good matching of the fibers and reinforcement of the joint. Special care was taken to get a tight joint by applying gentle pressure during hardening.

All fibers were tested for light transmission using a monitored UV-lamp. The fibers with lowest transmission were discarded (10%) resulting in a spread of 12% for the remaining fibers.

2.2 Light yield measurement

The absolute light yield for minimum–ionising particles was measured in a cosmic ray telescope with an effective area of 12 x 12 cm^2. The PMT pulse was integrated by a LeCroy 2249A ADC, triggered by a threefold coincidence of the signals from the cosmic trigger[§]. The ADC gate length was 100 ns. Figure¡ 1 shows the response to cosmic ray particles for the final tile/fiber/PMT layout.

The ratio of triggers with no signal above pedestal recorded in the ADC to the total number of triggers is equal to (0.37±0.03%), taking into account the trigger efficiency. From this we obtain an absolute light yield of 5.6±.1 photoelectrons.

2.3 Uniformity measurement

The tile uniformity was measured with a collimated ^{106}Ru source, a computer-controlled x-y scanning table as scintillator support and an XP2020 photomultiplier. The ADC was triggered by a

[‡]BICRON BC600 Optical Cement

[§]The absolute trigger efficiency was determined to be 98.9%

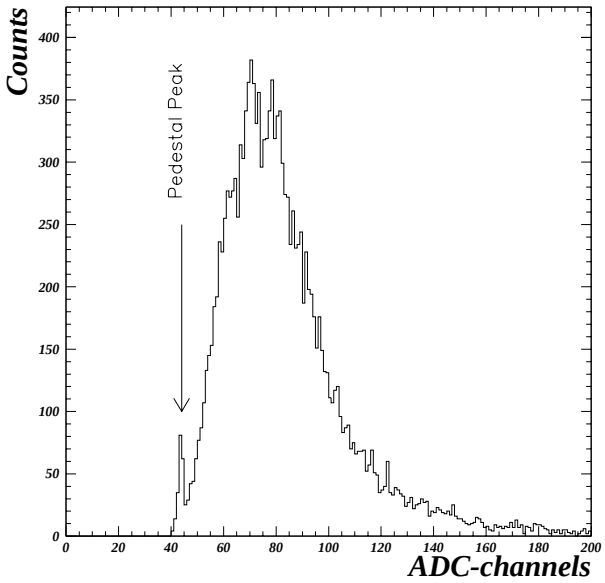

Figure 1: *Response of a scintillator tile to cosmic muons. The peak around the pedestal value of 45 ADC counts is due to false triggers and zero response due to photostatistics.*

coincidence of two photomultiplier signals reading out a large trigger counter located underneath the tile to be tested (figure 2). To ensure that the ^{106}Ru source simulates minimum–ionising particles, we measured the light yield of the tile also with the cosmic telescope. The pulse height spectra of cosmic muons and electrons from the ^{106}Ru source are very similar in shape, with peak values equal within 5%. A 3–mm–diameter collimator was used to measure the response over a 20 x 20 cm^2 tile in steps of 2 mm in x and y. The response is uniform within 5%.

The distribution of the mean values of the measurements for all positions is shown in figure 3. The slight bump below 120 channels is an effect occurring near the edge of the tile where some particles leave the tile before crossing its full thickness.

3 Mechanical layout

3.1 Tile assembly

The scintillator tiles are assembled in cassettes, made of 0.4 mm thick stainless steel; they are 20 cm wide and vary in length, containing between 1 and 10 tiles. In order for the readout fibers to clear the neighboring scintillator tile the 5 mm thick tiles are raised at the readout end, supported by a 2.5 mm thick rohacell strip. The total thickness of the cassette is $\simeq$ 11 mm and represents about 5 % of a radiation length (1.2 % for the scintillator and 4 % for the stainless steel). The length of readout fibers is $\simeq$ 300 cm. The six readout fibers of one tile are glued together in a connector

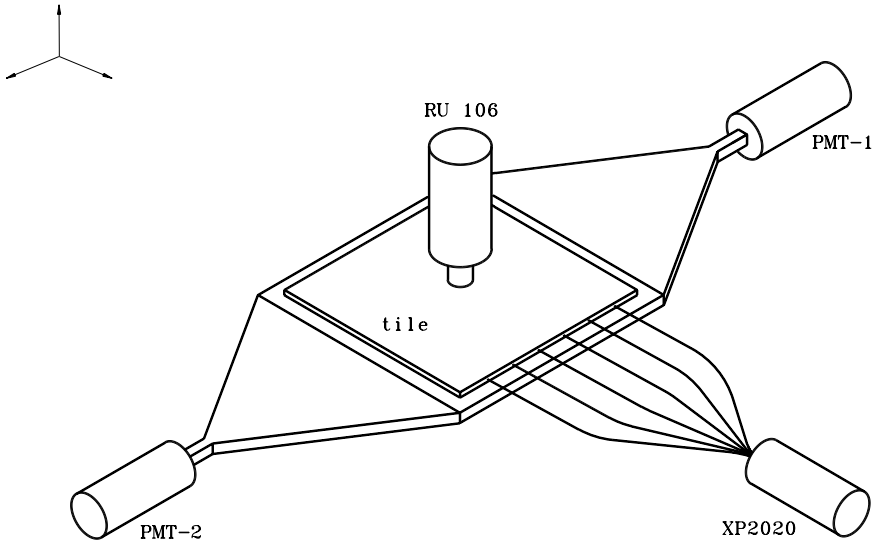

Figure 2: *Scanning table uniformity measurement*

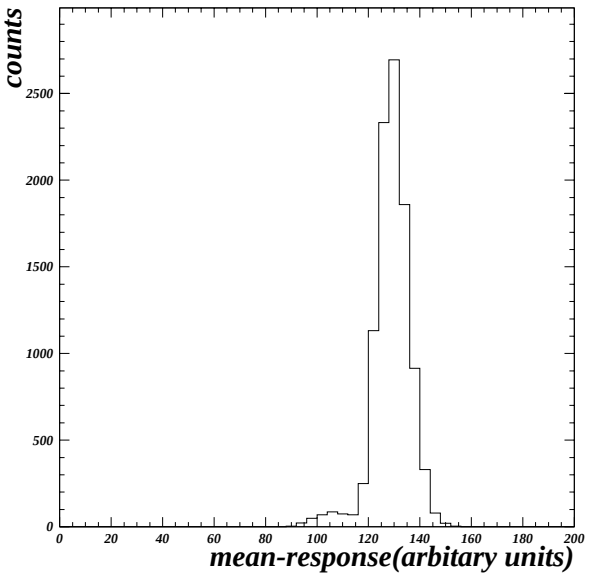

Figure 3: *Spread of response over a tile. The response is uniform within 5%.*

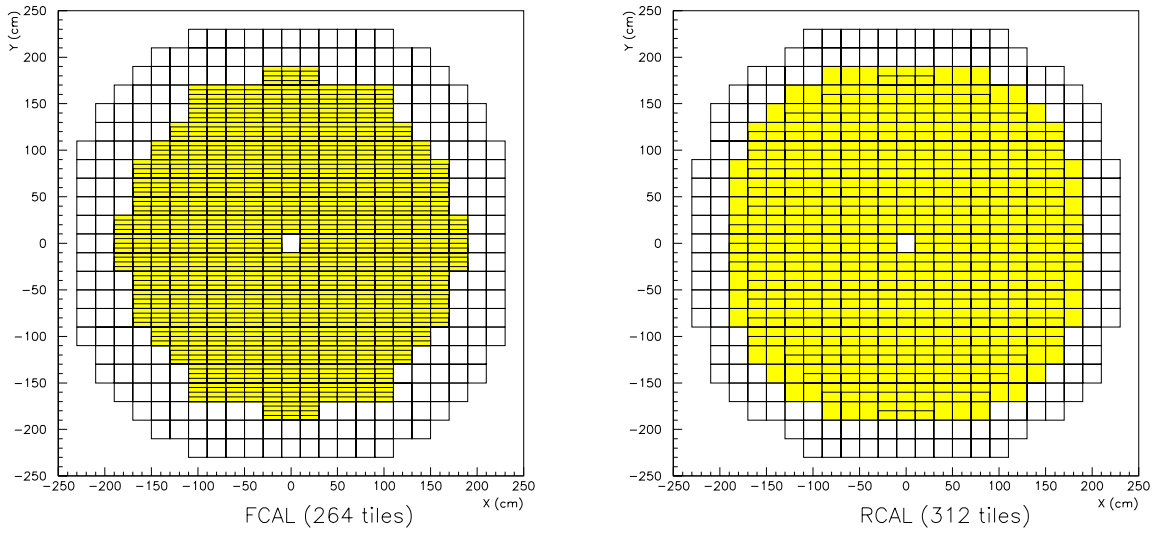

Figure 4: *Front view of the forward (FCAL) and rear calorimeter (RCAL). The 20 x 20 cm^2 white square in the center corresponds to the hole for the beam pipe. The coverage of the presampler is indicated by the shaded region.*

which is fixed to the PMT housing. In addition to the six fibers a seventh clear fiber is added to guide the light from a laser/LED system to the PMT.

3.2 Detector assembly

The forward and rear calorimeters are split in two halves, such that they can be withdrawn from the beam pipe region during injection of the electrons and protons in HERA. A group of 19 cassettes, which covers one half of each calorimeter face, is glued on a 2 mm thick aluminium plate (0.02 radiation lengths) of 2 x 4 m^2.

Figure 4 shows the coverage of the calorimeter by the presampler. Shown is the segmentation of the electromagnetic sections, which is finer in the region not shadowed from the nominal interaction point by the barrel calorimeter. The 20 x 20 cm^2 towers covered by the presampler tiles are shaded.

A 2.5 mm diameter tube is glued over the full length on the outside of each cassette, positioned at the center of the tiles. The tube guides a radioactive source for calibrating the light output of the individual tiles and the gain of the PMT channels (see section 7.2).

4 Photomultiplier tests

4.1 Performance specifications

Due to the limited space available in the ZEUS detector it was decided to use multichannel PMT's. The magnetic field amounts to a few hundred Gauss in the area where the PMT's are located and therefore adequate shielding is needed. Since we measure pulse heights, the crosstalk between adjacent channels in the tube is required to be less than 5%. Another requirement is the size of the photocathode for a single channel, which must match the readout fibers of one scintillator tile.

The Hamamatsu R4760 16-channel photomultiplier has been extensively tested for our application (see also [3]). This is a 4 x 4 multichannel PMT with a front face of 70 mm diameter. Each of the 16 channels has a 10 stage dynode chain, but they all share the same voltage divider. The diameter of the photocathode for each channel is 8 mm. Our PMT's fulfill the following requirements:

- cathode sensitivity > 45 μA/lm
- minimum gain at 1000 V: 1 x 10^6
- gain spread between channels, within one PMT assembly, less than a factor of 3

The crosstalk has been measured to be less than 3%.

4.2 HV supply and linearity measurement

A high voltage system based on the use of a Cockcroft–Walton generator has been developed [4]. Power dissipation is negligible compared to that of a resistive voltage divider. The system can be safely operated because of the low voltage input and provides a protection against high currents (light leaks); the maximum anode current is 100μA. The HV units consist of a microprocessor board and the voltage multiplier boards. The microprocessor performs the HV setting and monitoring.

The R4760 PMT operates in the range 800-1200V. Tests showed that the optimum linearity is obtained (at the cost of a slightly lower gain) if the dynode voltage differences are distributed in the proportions 2:1:1:1:1:1:2:2:4:3, starting at the cathode. Since a pulse height measurement is required, good knowledge of the relation between input charge and output signal is necessary. For the linearity measurement we used an LED and a linear neutral density filter. As an example we show in figure 5 the deviation from linear behaviour versus anode charge for a HV setting of 1100V. The dotted line shows the linear fit through the first four points, the dashed line represents a polynomial fit through the last four points. At an anode charge of 25 pC the measured values are about five percent lower than expected for linear behaviour. These values vary strongly from channel to channel and from PMT to PMT.

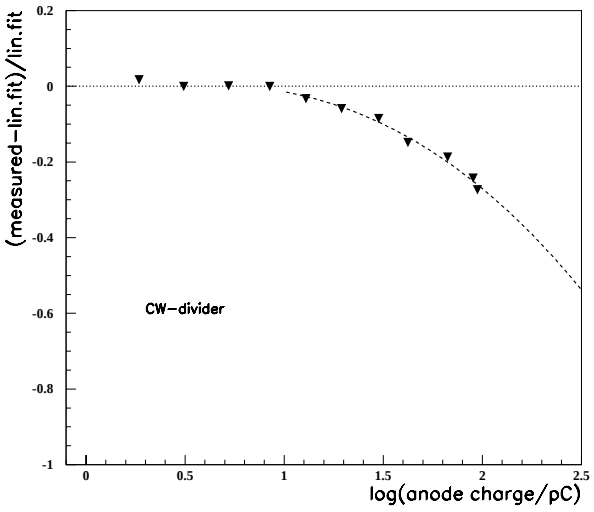

Figure 5: *Results on the PMT nonlinearity. The line shows the linear fit through the first four points. The dashed line represents a polynomial fit through the last four points.*

5 Readout system

The readout system is a copy of the existing ZEUS calorimeter readout system with some minor modifications [5]. The PMT pulses are amplified and shaped by a pulse shaper circuit mounted at the detector. The shaped pulse is sampled every 96 ns (the bunch crossing rate of the HERA storage ring) and stored in a switched capacitor analog pipeline. After receipt of a trigger from the ZEUS detector, eight samples are transferred from the pipeline to an analog buffer and multiplexed to ADCs. The data are sent to a location outside the detector where the digitisation and signal processing takes place. The modifications consist of upgraded versions of the shaping/amplifier [10] and the digital signal processor and a different mechanical layout of the analog front end cards.

6 Results from cosmic ray measurements

A cosmic ray test was performed to measure the light yield of the 576 tiles (264 FCAL and 312 RCAL tiles) assembled in 76 cassettes. The trigger system consists of eight cosmic ray telescopes. Each of these consists of two scintillator pads, 20 cm apart, with an area of 12 x 12 cm^2 which give, together with a third scintillator counter of 240 x 12 cm^2, a trigger system with a three-fold coincidence. The efficiency of each single telescope was better than 98%. The readout PMT was a 16-channel R4760 as used in the final presampler design. The setup allows the measurement of 16 channels simultaneously (e.g. two cassettes with eight tiles each). The trigger rate of the complete

setup was about 50 counts/min with about 6 counts/min for a single telescope. An example of the cosmic-test measurement is given in figure 1. To compare the light yield of different tiles, all 16 channels of the PMT were calibrated with a reference tile to correct for differences in quantum efficiency (QE) and gain between the 16 PMT channels. Figure 6 shows the mean value for all 576 tiles normalized to one of them. From the RMS value of the distribution we conclude that the responses of all tiles are equal to within 12%.

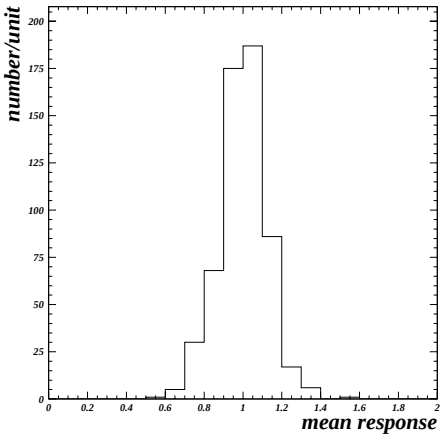

Figure 6: *Average pulse height for cosmic muons normalized to one after having corrected for the gain differences between individual PMT channels.*

Figure 7 shows the mean number of photoelectrons for each tile assuming a QE of 8.5% which is the minimum value accepted for the presampler PMT's (the mean QE for all channels is 11.6%).

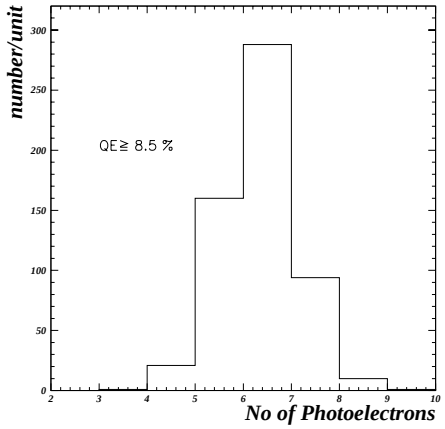

Figure 7: *Average number of photoelectrons per tile per MIP*

7 Calibration tools

7.1 Minimum–ionising particles in situ

During the operation of ZEUS, halo muons and charged hadrons are used to determine the response to single particles for each individual channel. The high voltage setting common to the sixteen pixels of one R4760 PMT is chosen such that the pixel with the least gain has an average response to minimum–ionising particles which is a factor of ten greater than the RMS noise level of the analog signal–processing front–end electronics (0.05 pC). The pixel–to–pixel gain variation of about a factor of three within one PMT results in a similar variation in the saturation levels. The in situ calibration for the 1995 running period achieved a precision of better than 5% per tile.

7.2 The radioactive source system

We use an LED/laser system to monitor the gains of the PMT's and a source system to monitor the combined response of tile, fiber and PMT. The response to a ^{60}Co source provides a relative calibration and quality control of the individual channels of the presampler. The source scans take place during shutdowns of HERA and provide information on the long term behaviour of the light output of the combination of scintillator and wavelength-shifting fiber.

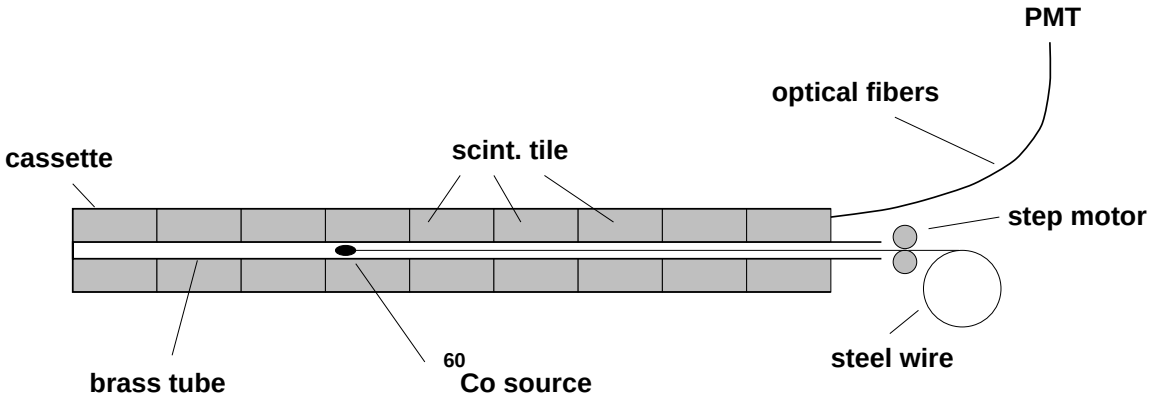

Figure 8: *Example of a cassette with 9 scintillating tiles and source tube glued on top, connected to source scanning system.*

Brass tubes with 2.5 mm outer diameter and 0.2 mm wall thickness run over the full length of the cassette, positioned in the middle (figure 8). They guide the pointlike (0.8 mm diameter, 1 mm length, 74 MBq) source. The source is driven in 2 mm steps via a 1.2 mm diameter steel wire by a stepper motor [6] controlled by a PC. The PMT currents are integrated with a time constant of 24 ms and read into a 16-channel 12-bit ADC card.

Figure 9 shows as an example the superposition of the responses of the tiles within one cassette

as a function of the location of the source. The different heights of the maxima are mainly due to the different gains of the 16 channels of the R4760 PMT, all supplied with the same high voltage. The ^{60}Co source is not collimated, as can be seen in the shape of the individual peaks.

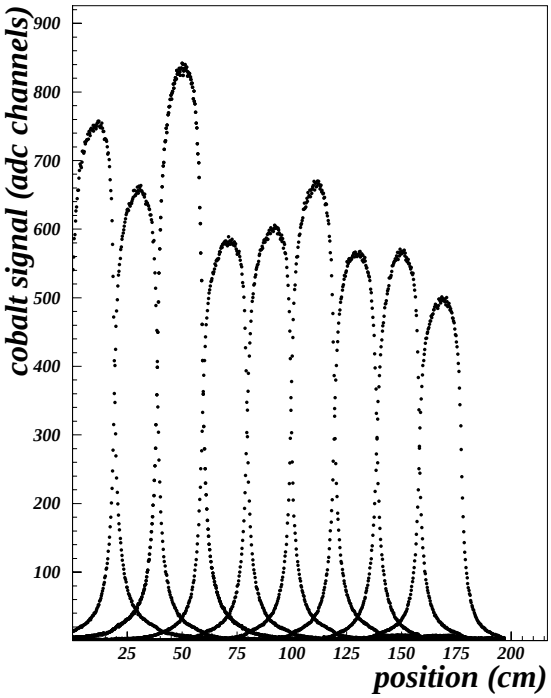

Figure 9: *Responses of the scintillating tiles within one cassette to a ^{60}Co source. The step width is approximately 2 mm.*

8 Beam test results

The influence of material in front of the ZEUS calorimeter on its energy measurement has been studied previously in several test beam runs with the ZEUS forward calorimeter (FCAL) prototype [7]. The corrections to the calorimetric measurements that can be derived from presampling measurements have been studied in subsequent test periods for both hadrons and electrons [8]. In the following we summarize the most recent results obtained for electrons with the final presampler design [9].

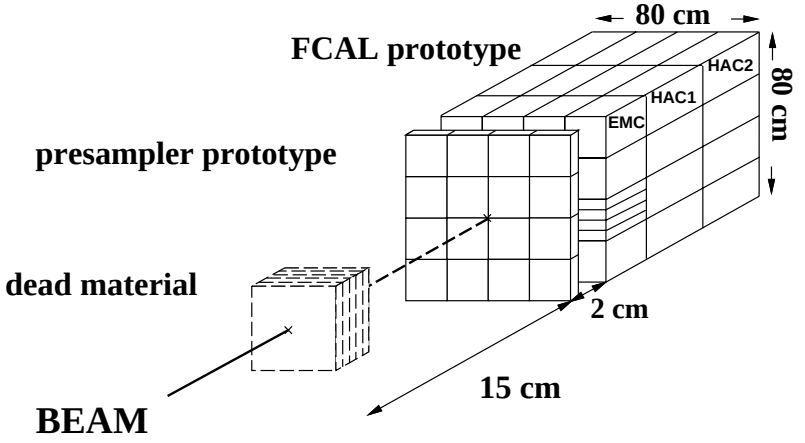

Figure 10: *Experimental setup of the FCAL prototype and presampler in CERN test beam. The presampler is mounted directly on the FCAL frontplate.*

8.1 Overview

The presampler prototype consists of an array of 4 x 4 scintillator tiles covering an area of 80 x 80 cm^2. As shown in figure 10 it is positioned directly in front of the ZEUS FCAL prototype which has the same lateral size. The depth of the calorimeter is 7 interaction lengths [7]. Beam tests were performed in the X5 test beam of the CERN SPS West Area. The prototype presampler detector is read out via an R4760 multichannel photomultiplier using the Cockcroft–Walton HV system. Furthermore, the final readout electronics was used for both the presampler and the FCAL prototype modules.

The uranium radioactivity was used to set the relative gains of the calorimeter phototubes and 15 GeV electrons served to set the energy scale. Muons were used to calibrate the presampler. The combined response of the presampler and calorimeter was determined for electrons in the energy range from 3-50 GeV. The amount of material installed in front of the presampler varied between 0 and 4 radiation lengths (X_0) of aluminium. During these studies, the position of both calorimeter and presampler relative to the beam was fixed. A delay wire chamber allowed the determination of the impact point of the beam particles with an accuracy of 0.5 mm.

Most of the data were recorded with a defocussed beam about 10 cm in diameter, facilitating studies of uniformity and position dependence of the energy correction algorithms.

8.2 The uniformity of the presampler response to muons

Figure 11 shows the mean presampler response to 75 GeV muons. The position information was provided by the delay wire chamber. The presampler signals for the incident muons are normalized to the response at the center of the tile and averaged over uniformly populated rectangles of 90 x 5 mm^2. The nonuniformity in the sum of the two bordering tiles is a few percent in the regions of the fibers. In the horizontal direction (figure 11b) the tiles are mounted within one cassette with no gaps between them. In the vertical coordinate (figure 11c) a signal drop is observed between the cassettes due to the 1.4 mm gap between the scintillator tiles. The nonuniformity averaged over the surface of a tile is less than 1%.

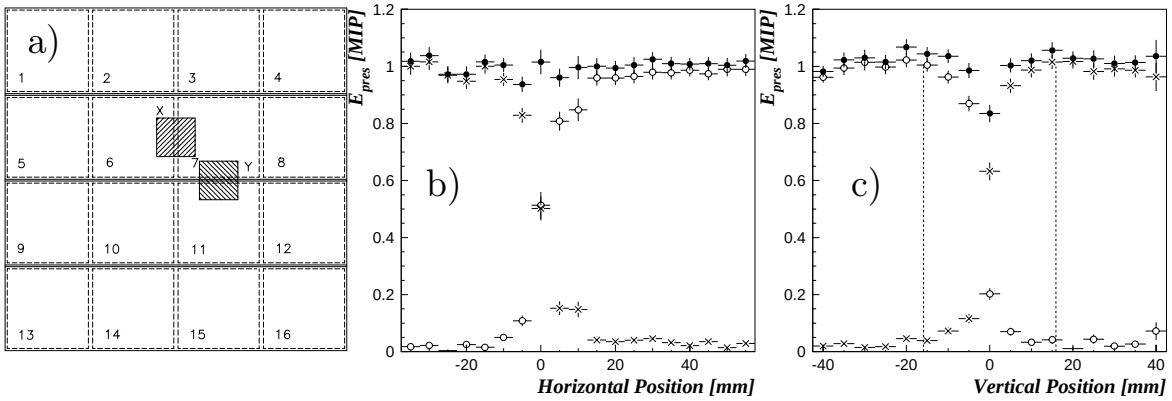

Figure 11: *The muon response uniformity of the presampler near tile borders. a) A sketch of scanning region, b) a horizontal scan (* represents the response of tile 6, ∘ that of tile 7 and • the sum of both), c) a vertical scan, perpendicular to the embedded fibers. The dashed lines indicates the fiber positions. The data in both plots are averaged over a uniformly populated rectangle 90 x 5 mm^2 in area with the long side perpendicular to the scanning direction.*

8.3 The presampler response to electrons

The electron beam used for the energy correction studies was 1 cm wide and 10 cm high, centered horizontally within one FCAL module and vertically on one of the 20 x 5 cm^2 electromagnetic sections. The presampler signal (E_{pres}) was obtained by summing all 16 tiles in order to be sure to get the entire signal and because the electronic noise contribution was negligible. The signal from

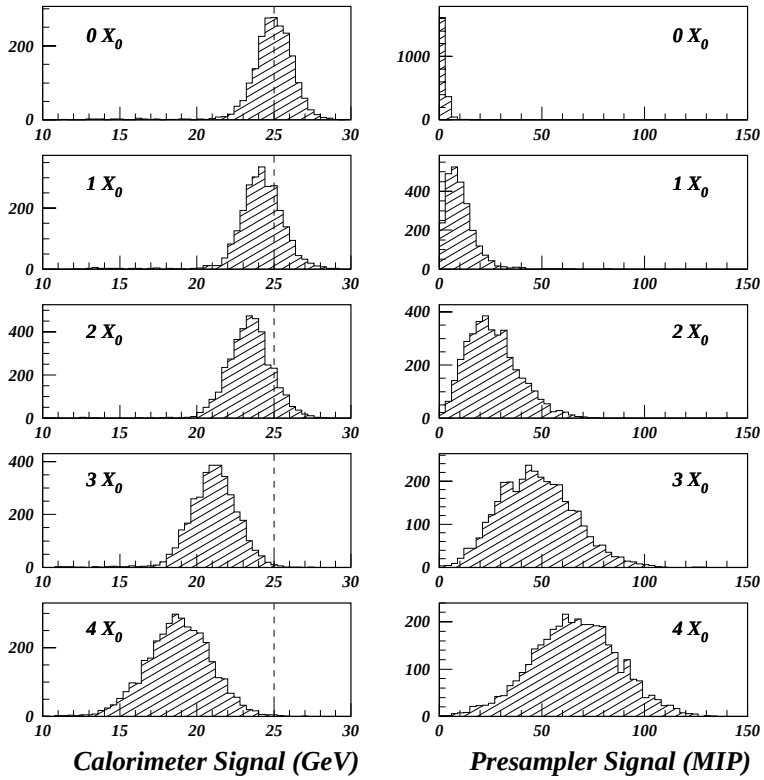

Figure 12: *Signal distributions in the calorimeter and presampler for 25 GeV electrons having passed through 0, 1, 2, 3, and 4 radiation lengths of aluminium absorber.*

each tile was normalized to its average response to muons, resulting in units we refer to as "MIP". Aluminium plates of 3 cm thickness were used as the absorber material. In the following three such plates together are referred to as one radiation length, an approximation which is accurate to 1%.

As examples of the calorimeter and presampler signal spectra we show in figure 12 the energy distributions measured with the calorimeter (E_{cal}) and the signal in the presampler for 25 GeV electrons for aluminium absorber thicknesses ranging between 0 and 4 X_0. The mean value for E_{cal} decreases by more than 20% but the shapes of the distributions remain approximately gaussian. The resolution deteriorates substantially in the presence of more than 2 X_0 of absorber material.

Table 1 shows the relative calorimeter signal loss and the average and RMS values of the presampler signal spectra for the full range of electron energies and absorber thicknesses. The uncertainties presented are dominated by the statistical precision.

Energy (GeV)	Absorber (X_0)	Rel. Energy Loss (%)	Presampler Avg (MIP)	Presampler RMS (MIP)
3	1	7.8 ± 1.0	5.5 ± 0.1	3.7 ± 0.1
	2	18.0 ± 1.0	10.3 ± 0.2	5.3 ± 0.1
	3	32.8 ± 1.0	12.0 ± 0.2	5.6 ± 0.1
	4	49.4 ± 1.0	12.1 ± 0.2	5.5 ± 0.1
5	1	6.4 ± 0.6	6.2 ± 0.2	4.1 ± 0.1
	2	13.0 ± 0.7	12.8 ± 0.2	6.5 ± 0.2
	3	27.4 ± 0.7	16.9 ± 0.3	7.3 ± 0.2
	4	42.5 ± 0.7	19.5 ± 0.3	7.1 ± 0.2
10	1	4.8 ± 0.5	7.7 ± 0.2	5.0 ± 0.1
	2	10.1 ± 0.5	18.2 ± 0.4	8.9 ± 0.3
	3	20.3 ± 0.5	27.4 ± 0.4	10.9 ± 0.3
	4	34.6 ± 0.7	32.7 ± 0.6	11.3 ± 0.4
15	1	3.5 ± 0.4	7.9 ± 0.2	5.2 ± 0.2
	2	7.8 ± 0.4	20.4 ± 0.5	9.6 ± 0.4
	3	17.3 ± 0.4	34.9 ± 0.6	13.8 ± 0.4
	4	29.6 ± 0.6	46.0 ± 0.8	14.6 ± 0.6
25	1	2.7 ± 0.3	9.8 ± 0.2	6.5 ± 0.2
	2	5.9 ± 0.3	26.6 ± 0.4	12.8 ± 0.3
	3	15.4 ± 0.3	47.3 ± 0.5	17.9 ± 0.4
	4	24.4 ± 0.3	66.1 ± 0.6	20.9 ± 0.4
50	1	1.6 ± 0.2	12.0 ± 0.3	7.9 ± 0.2
	2	4.6 ± 0.2	35.6 ± 0.6	16.4 ± 0.4
	3	11.5 ± 0.5	72.7 ± 2.1	27.7 ± 1.5
	4	19.8 ± 0.3	108.1 ± 1.2	31.6 ± 0.8

Table 1: *The relative decrease in the calorimeter signal and the average and RMS values of the presampler signal spectra for each electron energy and each aluminium absorber thickness used in the test beam studies. The uncertainties shown are dominated by the statistical precision.*

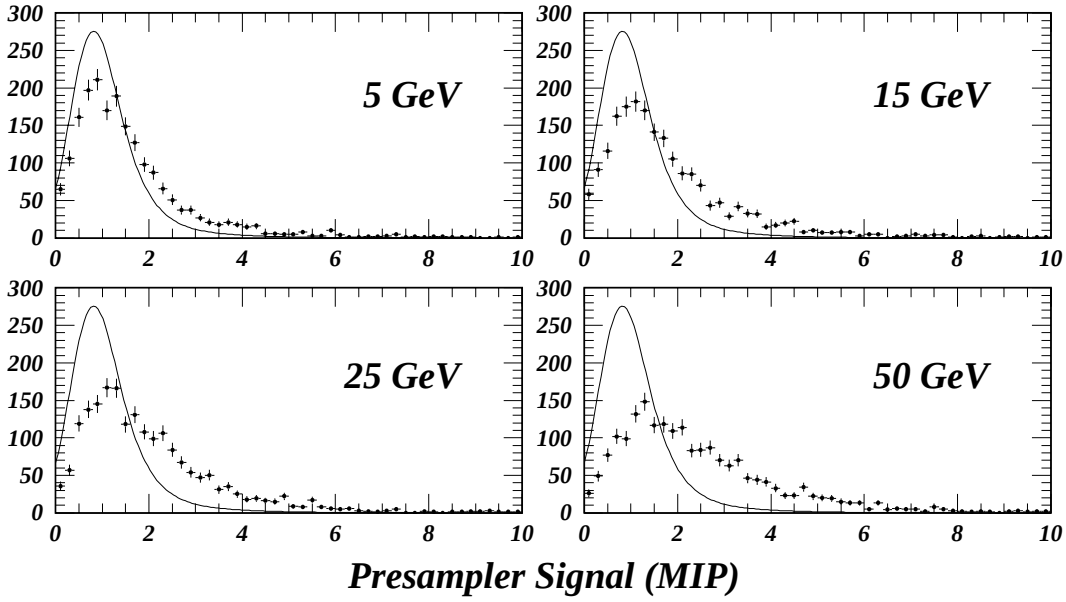

Figure 13: *A comparison of the presampler signal spectra for 5, 15, 25, and 50 GeV electrons to that for muons. The smooth curve shows the response to muons. The presampler signal has been normalized to the average value of the muon spectrum. Each spectrum contains 2000 entries.*

8.3.1 Contribution of backscattering to the presampler signal

The comparison of presampler signal spectra from incident muons with those of incident electrons allowed us to estimate the contribution of backscattering from the electromagnetic showers in the uranium calorimeter. Figure 13 shows this comparison for 5, 15, 25 and 50 GeV electrons. We determine the average relative increase to be 1.45, 1.65, 1.80, and 2.16 respectively, to an accuracy of 2%. By adding absorber upstream of the presampler and displacing both absorber and presampler several meters upstream to measure the decreased contribution from backscattering, we ascertained that the backscattering contribution is not increased by the presence of the absorber in front of the presampler. Thus we can be sure that the backscattering contribution remains at the level of 1 MIP and can be neglected at the level of 10% of the size of the signals we use for the electromagnetic energy correction. We also measured the backscattering contribution from hadronic showers and found for 15 and 75 GeV incident pions values for the average relative increase less than 1.5 and 2.0 respectively.

8.3.2 Electron energy correction

Figure 14 shows the correlation between the presampler signal (normalized to the average signal of a minimum–ionising particle) and the calorimeter signal for 25 GeV electrons as a function of the amount of absorber material.

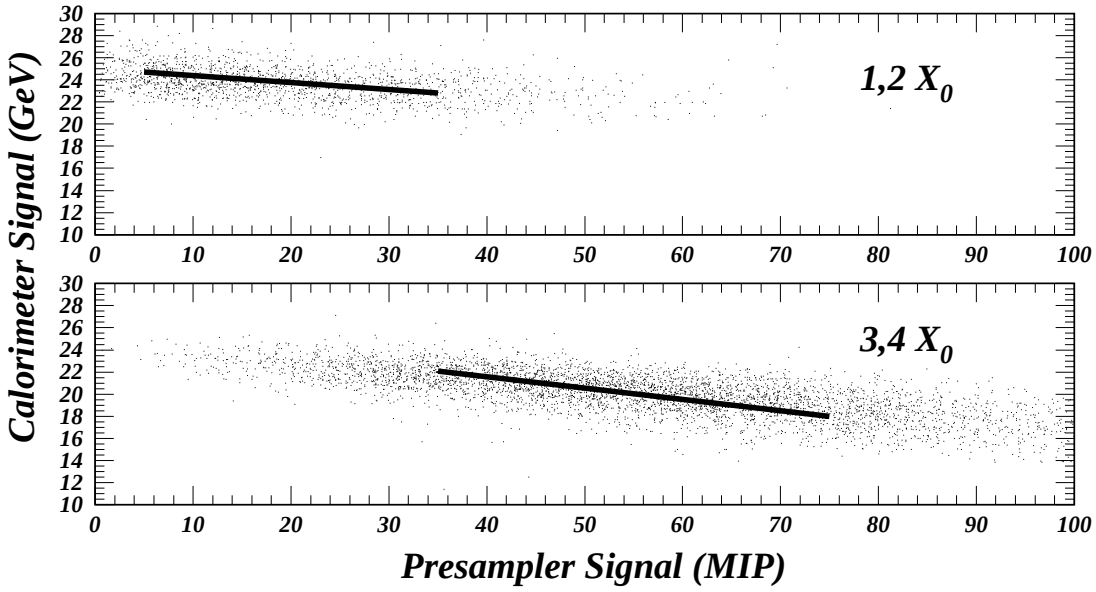

Figure 14: *Calorimeter versus presampler response for 25 GeV electrons and absorber material ranging from 1 to 4 X_0. The line represents the fit to the data according formula (1).*

We have considered a variety of parametrisations for the relationship between calorimeter and presampler responses. In the well–defined environment of a test beam the correction is straightforward and depends on the incident energy and the amount of absorber material, both of which are precisely known.

In a detector environment the amount of absorber material in front of the calorimeter is not uniformly distributed, arising from cables, support structures, etc. One can, however, identify regions where the average amount of absorber material is roughly known. For this reason we show here the result obtained with one set of correction constants common to the 1 and 2 X_0 data set and one for the 3 and 4 X_0 data set. The relation between the measured mean values of E_{cal} and E_{pres} has been parametrised in a linear approximation:

$$E_{cal} = a_0 + a_1 E_{pres} \tag{1}$$

The result for the two data sets for 25 GeV electrons is shown in figure 14. The parameters a_i depend on the amount of material and on the electron beam energy. This correction algorithm allows for a linear energy dependence of the parameters a_i: $a_i = \alpha_i + \beta_i E_{beam}$. We neglect the dependence on the amount of absorber material in order to estimate the success of the algorithm when the amount of absorber varies within the data sample. The parameters α_i and β_i are determined by minimising the difference of the beam energy and the corrected calorimeter signal,

The results for the corrected calorimeter response for electrons in the energy range 3-50 GeV, are shown in figure 15. This procedure provides a correction accurate to 3% for the energy range

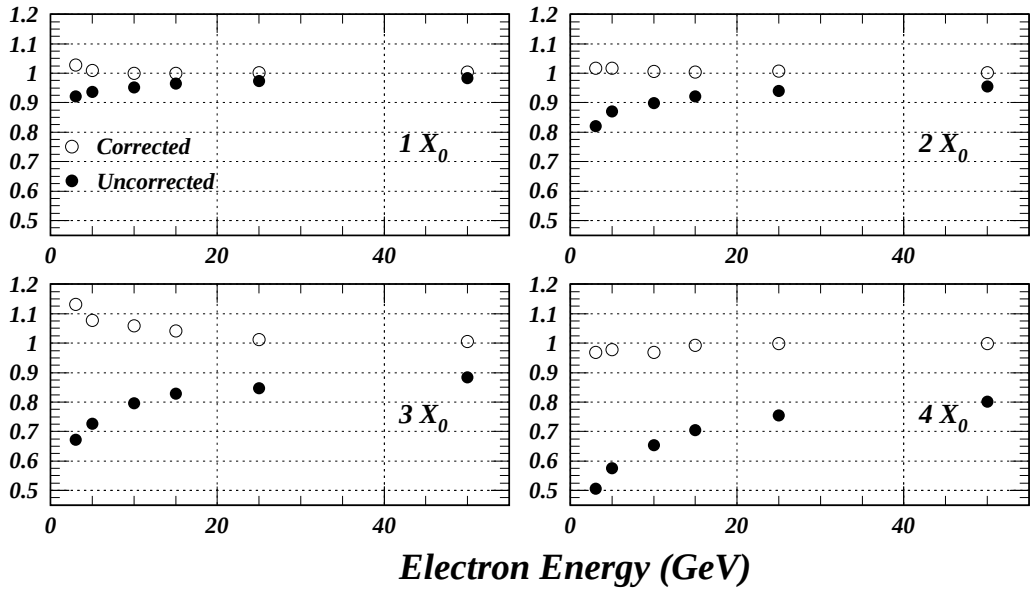

Figure 15: *Average calorimeter response normalized to the electron energy versus the electron energy before and after correction*

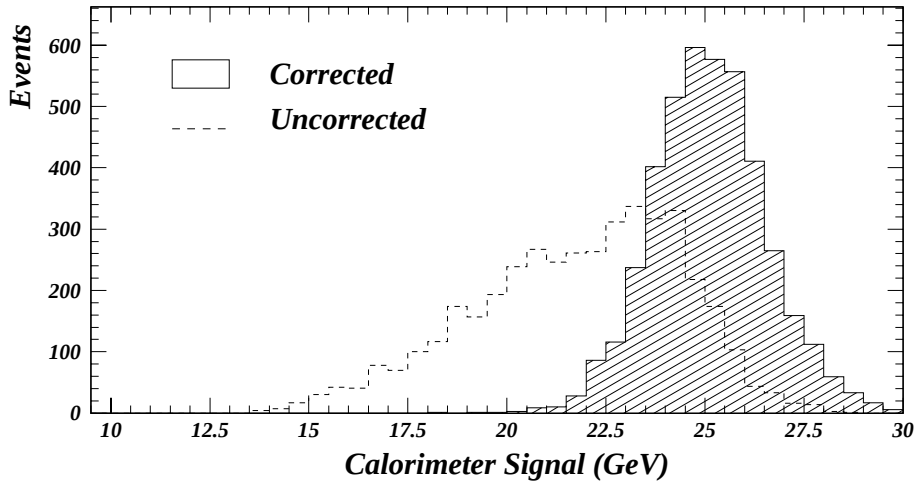

Figure 16: *Reconstructed energy distributions for 25 GeV electrons for a mixture of the 1-4 X_0 data before and after application of the correction algorithm*

studied here, but for an overcorrection of about 10% for the 3 X_0 data points at low energy. For electron energies greater than 5 GeV and for absorber thickness less than 2 X_0, the values relevant to the operation of the ZEUS detector, this simple correction algorithm yields a systematic precision of 2%.

The improvement in the energy resolution as well as in the energy scale is shown in figure 16. The energy distribution of 25 GeV electrons for a merged 1-4 X_0 data set is shown before and after correction.

9 Summary and conclusions

We have designed, built, installed and operated a scintillator-tile presampler for the forward and rear calorimeter of the ZEUS detector. The scintillation light from the tiles is collected by wavelength-shifting fibers and guided to multi-anode photomultipliers via clear fibers. The signals are shaped, sampled and pipelined in the manner employed for the calorimeter itself, easing the integration of the presampler in the ZEUS data acquisition system. The performance of the tiles and fiber readout were monitored with a cosmic–ray telescope and with collimated sources during production. The single-particle detection efficiency is greater than 99% and the response uniformity over the area of each of the 576 20 x 20 cm^2 tiles is better than 5%. An LED flasher system and scans with radioactive sources have proven useful diagnostic tools since the installation of the presampler. The in situ calibration with minimum–ionising particles during the 1995 data–taking period achieved a precision better than 5% per tile. Test beam studies of a presampler prototype with the final geometry and readout in combination with a prototype of the ZEUS forward calorimeter verified the efficiency and uniformity results and allowed the determination of backscattering contributions. Tests with electrons were performed in the energy range 3–50 GeV with 0–4 radiation lengths of aluminium absorber. These studies have proven the feasibility of an electron energy correction accurate to better than 2% in the energy range and for the configuration of inactive material relevant to the ZEUS detector.

10 Acknowledgements

We would like to thank the technical support from the institutes which collaborated on the construction of the presampler, in particular W. Hain, J. Hauschildt, K. Loeffler, A. Maniatis, H.–J. Schirrmacher (DESY), W. Bienge, P. Pohl, K.–H. Sulanke (DESY–IfH Zeuthen), M. Gospic, H. Groenstege, H. de Groot, J. Homma, I. Weverling, P. Rewiersma (NIKHEF), R. Mohrmann, H. Pause, W. Grell (Hamburg), M. Riera (Madrid), R. Granitzny, H.–J. Liers (Bonn). We are also grateful for the hospitality and support of CERN, in particular the help of L. Gatignon is much

appreciated. Finally we would like to thank R. Klanner for his enthusiastic support during all phases of the project.

References

[1] The ZEUS Detector, Status Report, DESY (1993).

[2] A. Andresen et al. Nucl. Instrum. Methods **A309** (1991) 101.

[3] A.Weisenberger et al., Nucl. Instrum. Methods**A327** (1993) 500.

[4] *A Remote–Controlled High Voltage system for PMT's.* M.Gospic, H.Groenstege, NIKHEF-ETR 94-11
http://www.nikhef.nl/www/pub/et/zeus/presampler/presampler.html
L. Hubbeling, CERN-EP Internal report 78-5.

[5] A.Caldwell et al., Nucl. Instrum. Methods **A321** (1992) 356.

[6] B.Krebs et al., Nucl. Instrum. Methods **A323** (1992) 611.

[7] U.Behrens et al. Nucl. Instrum. Methods **A289** (1990) 115.
A.Andresen et al. Nucl. Instrum. Methods **A290** (1990) 95.
Studies of Particle Jets with an Interaction Trigger, W.Kröger, Ph.D. Thesis, University of Hamburg, 1992.

[8] *A Prototype Presampler for Uranium-Scintillator Calorimeter in ZEUS*, H.Grabosch et al., NIKHEF-H/93-11.

[9] *Calibration of the Presampler for the Electron Energy Measurement in the ZEUS Detector*, A.Bornheim, Diploma Thesis, Bonn IB 95-24 (1995) (in German)

[10] *Shaping Amplifier for PMT signals for ZEUS*, P.Rewiersma, I.Weverling, NIKHEF-ETR 94-12.

The Gas Electron Multiplier (GEM)

R.Bouclier, M.Capeáns, W.Dominik, M.Hoch, J-C.Labbé, G.Million, L.Ropelewski, F.Sauli and A.Sharma[a]

CERN, CH-1211 Genève, Switzerland

[a] VUB-ULB Brussels, Belgium

Abstract

We describe operating principles and results obtained with a new detector element: the Gas Electrons Multiplier (GEM) [1]. Consisting of a thin composite sheet with two metal layers separated by a thin insulator, and pierced by a regular matrix of open channels, the GEM electrode, inserted on the path of electrons in a gas detector, allows to transfer the charge with an amplification factor approaching ten. Uniform response and high rate capability are demonstrated. Coupled to another device, multiwire or micro-strip chamber, the GEM electrode permits to obtain higher gains or less critical operation; separation of the sensitive (conversion) volume and the detection volume has other advantages: a built-in delay (useful for triggering purposes), and the possibility of applying high fields on the photo-cathode of ring imaging detectors to improve efficiency.

Multiple GEM grids in the same gas volume allow to obtain large amplification factors in a succession of steps, leading to the realization of an effective gas-filled photomultiplier.

I. INTRODUCTION

Methods for obtaining large, stable proportional gains in gaseous detectors are a continuing subject of investigation in the detector's community. Several years ago, Charpak and Sauli [2] introduced the Multi-Step Chamber (MSC) as a way to overcome some limitations of gain in Parallel Plate and Multi-Wire Proportional Chambers (MWPC); two parallel grid electrodes, mounted in the drift region of a conventional gas detector and operated as parallel plate multipliers, allow to pre-amplify drifting electrons and transfer them into the main detection element. Operated with a photo-sensitive gas mixture, the MSC allows to reach gains large enough for single photon detection in Ring Imaging Cherenkov (RICH) detectors [3].

More recently, Charpak and Giomataris have developed MICROMEGAS, a high gain gas detector using as multiplying element a narrow gap parallel plate avalanche chamber [4]. With gaps in the range 50 to 100 μm, realized by stretching a thin metal micro-mesh electrode parallel to a read-out plane, the authors

have demonstrated very high gain and rate capabilities, understood to result from the special properties of electron avalanches in very high electric fields.

The major practical inconvenience of both described detectors lies in the necessity of stretching and maintaining parallel meshes with very good accuracy; the presence of strong electrostatic attraction forces adds to the problem, particularly for large sizes. This requires heavy support frames, and in the case of MICROMEGAS, the introduction in the gap of closely spaced insulating lines or pins with the ensuing complication of assembly and loss of efficiency.

An interesting device recently developed, the CAT (*Compteur A Trou* [5]), consists of a matrix of holes drilled through a cathode foil; with the insertion of an insulating sheet between cathode and buried anodes, it allows to guarantee a good gap uniformity and to obtain high gains.

In the present paper, we describe a novel concept that seems to hold both the simplicity of the MSC scheme, and the high field advantages of MICROMEGAS and CAT, however mechanically much simpler to implement and more versatile: the Gas Electron Multiplier (GEM).

II. PRINCIPLE OF OPERATION

The basic element of the GEM detector is a thin, self-supporting three-layer mesh realized by the conventional photo-lithographic methods used to produce multi-layer printed circuits. A thin insulating polymer foil metallized on each side is passivated with photo-resist and exposed to light through a mask; after curing, the metal is patterned on both sides by wet etching and serves as self-alignment mask for the etching of the insulator in the open channels. We have obtained medium size meshes (5 by 5 cm^2) with 25 μm thick polymer sandwiched between 18 μm thick copper electrodes; the etching pattern has rows of 70 μm wide holes spaced 100 μm (Fig. 1); the fabrication technology, developed by the CERN Surface Treatment Service[1], can be extended to larger areas.

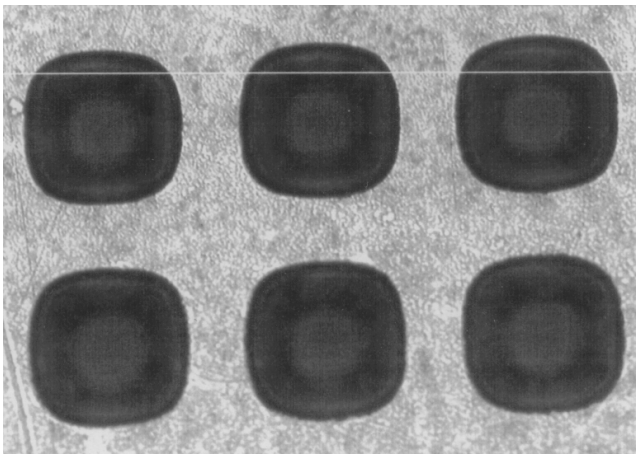

Fig. 1: Micro-photography of the three-layer (metal-insulator-metal) GEM grid. The distance betwen holes is 100 μm.

[1] R. De Oliveira, A. Gandi and L. Mastrostefano

Because of the etching process, holes are conical in shape from both entry sides, probably improving the dielectric rigidity (see Fig. 2). Upon application of a suitable difference of potential, the electric field in a channel of the GEM grid develops as shown in Fig. 2; for this calculation, the mesh has been inserted between two equidistant electrodes at symmetric potentials. From the data reported by the authors of Ref. 4, we expect to obtain multiplication in the high field in the center of the channel at a difference of potential around two hundred volts; for this value, the corresponding field strength along the central line is shown in Fig. 3: at the maximum, it reaches 40 kV cm^{-1}. Electrons produced by ionization in the upper gas volume drift into the channels, multiply in avalanche in the high field region and leave towards the electrodes in lower volume. Most of the ions generated in the avalanche recede along the central field lines, limiting the perturbing effects of the insulator charging up.

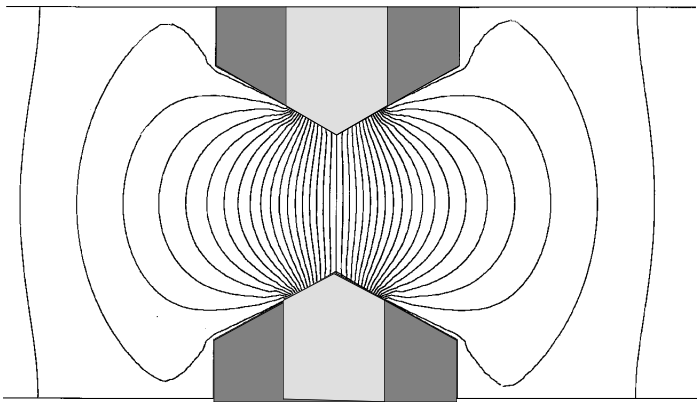

Fig. 2: Equipotentials lines in the GEM multiplying channel (V_{GEM} =200V).

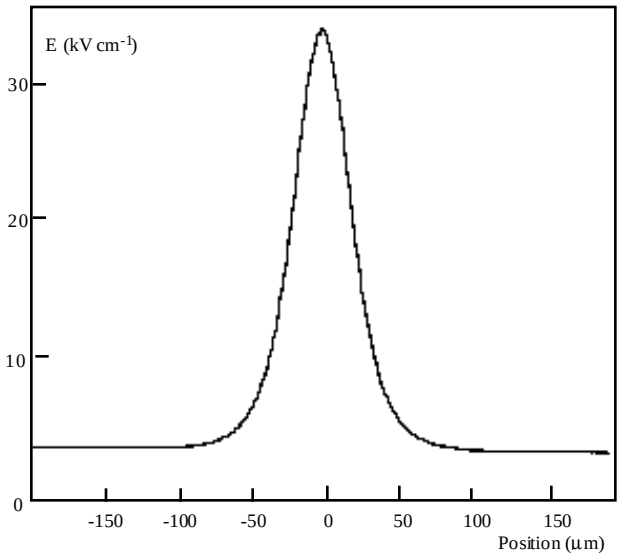

Fig. 3: Electric field along the central field line in the multiplying channel.

Thanks to the focusing effect of the field, one expects full efficiency for transfer of charge, and the dense channel spacing reduces image distortions. For the device to properly function, a good and regular insulation between the grid electrodes is required, with no sharp edges, metallic fragments or conducting deposits in the channel; this has been obtained by careful optimization of the etching and cleaning procedures. The first GEM mesh manufactured on our design had around a quarter million channels covering a square grid 50x50 mm^2, and was used for the measurements described in what follows. The test assembly is schematically shown in Fig. 4: a standard, small size MWPC is modified replacing one cathode with a thin printed circuit board holding the GEM mesh in the center; the mesh is pasted to the board, taking great care to avoid problems at the outer edge of the print (the metal on one side of the grid was removed for a few mm along the edges). Above the GEM electrode, a second cathode (the drift electrode) defines the sensitive volume of the detector.

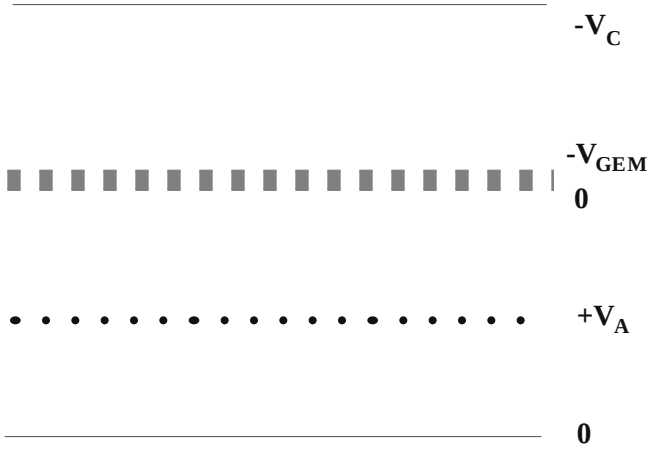

Fig. 4: Test assembly with the GEM multiplier mounted within a standard MWPC (drawing not to scale).

For convenience, the MWPC is operated with the anode wires at positive potentials, the signals being picking up through HV decoupling capacitors; this choice allows to maintain the lower electrode of GEM at ground potential, and easily increase the multiplying voltage. For ionization produced in the MWPC gaps, a regular process of collection and amplification takes place; electrons released in the upper drift region, on the contrary, can drift into and through the GEM channels and multiply, depending on potentials. Using a collimated X-ray source, one can easily disentangle the operation in the two regions. For most of this study, we have used a 5.9 keV ^{55}Fe X-ray source; to measure the rate capability, the detector has been exposed to a collimated 8 keV beam from a generator.

III. EXPERIMENTAL RESULTS

A. Charge transfer and pre-amplification

In order to avoid having to reach excessive potentials across the GEM mesh, we have found convenient to operate the detector at low quencher levels; a good choice is a mixture of Argon and Dimethyl-ether (DME) in the proportion 90-10, used for all measurements described here. The detector operates however well in other mixtures, including some with the level of quencher below the flammability limit (3.5% for

DME). The MWPC is powered at a voltage providing a moderate gain (~10^4), keeping V_{GEM} grounded; the standard ^{55}Fe spectrum is recorded. With the upper drift electrode at fixed potential (typically -1 kV), the negative potential on GEM is progressively increased. At -V_{GEM}~ 50 V, a signal begins to appear, corresponding to charge transferred from the drift region; at ~ 140 V the transferred charge equals the direct one (100% transparency). Increasing -V_{GEM} further, the pre-amplified charge exceeds the direct component. Fig. 5 shows a typical pulse height spectrum, recorded at a pre-amplification factor around 6:

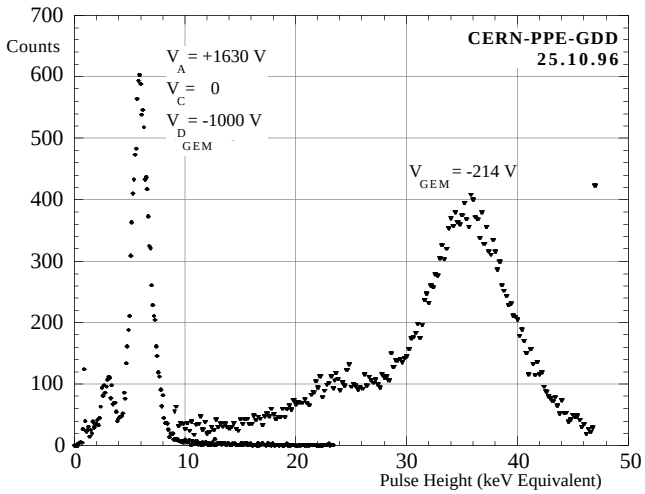

Fig. 5: ^{55}Fe pulse height spectrum recorded in the MWPC without (left) and with pre-amplification.

The energy resolution of the detector is not affected by the pre-amplification process; from Fig. 5 one can infer a resolution of around 11% r.m.s. for the pre-amplified charge, as compared to 12% r.m.s. for the direct signal (the apparent improvement is probably due to some non-linearity of the response)

Fig. 6 shows the measured pre-amplification factor, defined as the ratio of the most probable pulse height between transferred and direct spectra for the 5.9 keV line, as a function of the GEM voltage. In this particular mesh, the first to be realized, discharges appear at around -230 V; they are however without any consequence to the detector. From previous observations [6], we expect that use of a thicker insulator (50 to 100 μm instead of 25) could lead to higher effective gains.

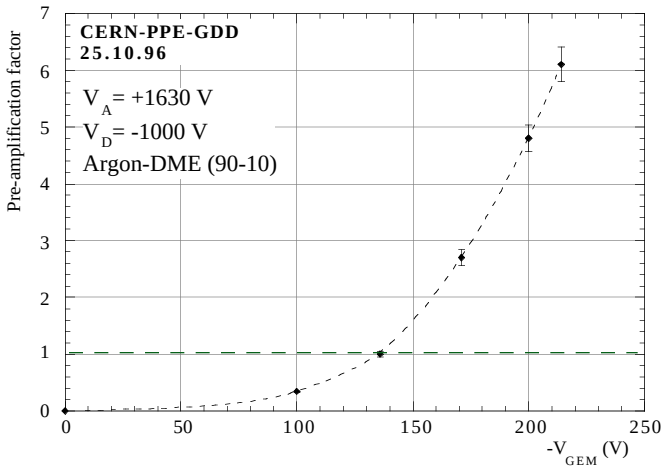

Fig. 6: Pre-amplification factor as a function of the difference of potential on the GEM grid.

The strength of the field in the drift region does not affect, in a wide range, the collection and transfer characteristics and the pre-amplification factor (although it affect other drift properties). We have seen no difference in transferred charge, at a pre-amplification factor around 6, varying the drift voltage from -500 to -2000 V. This can be exploited to tune drift velocity, diffusion and Lorentz angles according to experimental needs.

B. Uniformity of response

The uniformity of response of the detector has been measured by displacing the collimated source across the active area (50x50 mm^2); the gain is remarkably uniform (Fig. 7), with a maximum variation of ±4% (which includes the possible variations in the MWPC). Because of poor collimation of the source, the signal is detected on a slightly wider region than the opening of the grid.

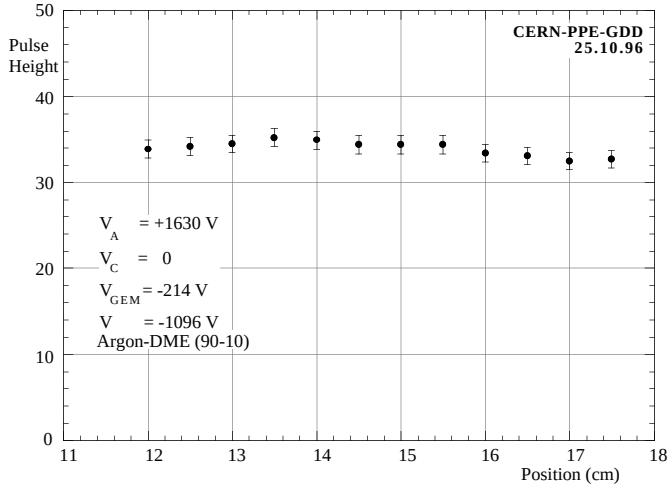

Fig. 7: Gain uniformity measured across the GEM grid.

C. Rate capability

To investigate possible gain reductions induced by charges deposited on the insulator surfaces within the channels, we have exposed the GEM detector to increasing rates of 8 keV X-rays from a generator. The irradiated area covered about 3 mm^2. It should be noted that the MWPC itself (with 2 mm wire spacing) is expected to suffer space charge gain drops at rates exceeding ~ 10^4 $mm^{-2}s^{-1}$. In order to be in similar conditions, the measurements were realized at constant total gain adjusting the MWPC anode potential. The preliminary results, Fig. 8, show no difference in behavior implying the absence of charging up processes in the GEM mesh.

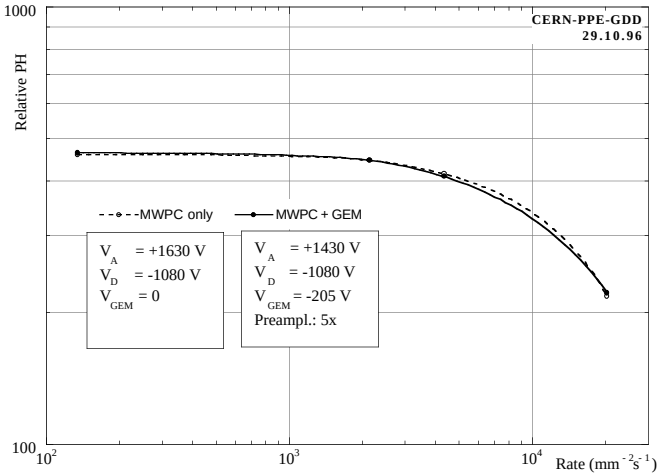

Fig. 8: Gain as a function of rate measured at equal gain for the MWPC and for the GEM+MWPC chamber.

Coupled to a high-rate detector, such as the MSGC, the rate capability of GEM may be limited by charging-up of the insulator in the open channels. If such is the case, it can be envisaged either to use a moderate conductivity material for the layer (in the range 10^{10} to 10^{13} Ω.cm), or to coat the mesh by vacuum deposition or Chemical Vapor Deposition (CVD) with a thin controlled resistivity layer in the range 10^{14} to 10^{16} Ω/q, using technologies developed for MSGCs [7].

IV. APPLICATIONS

A variety of uses can be envisaged for the GEM mesh: self-supporting, the element can be easily incorporated in other structures. The added pre-amplification factor, even moderate, can ease the operation of any gain-critical detector.

In Micro-Strip Gas Chambers (MSGC) a serious problem of discharges has been met recently [8,9]. When operated close to their maximum gain limit in order to efficiently detect minimum ionizing particles, MSGCs can be irreversibly damaged by a discharge initiated by heavily ionizing tracks (recoils produced by neutrons, nuclear fragments); the effect is enhanced in presence of a high flux of radiation, and its probability depends strongly on the operating voltage [10]. The use of a GEM grid above the MSGC, with even a moderate pre-amplification, would allow to operate the MSGC well below the critical potential for

discharges. The moderate increase in the spatial extension of the detected charge, with its de-clustering effect, should also improve the localization accuracy; the added delay, corresponding to the drift time of electrons from GEM to the MSGC plate, could be exploited for the first level triggering.

A second application of the pre-amplification principle, already mentioned, could be in fast RICH detectors. Aside for allowing larger gain and therefore easing single photo-electron detection, the structure can be designed to exert a high electric field on the solid photo-cathode side of the detector, thus substantially improving its quantum efficiency [11]. Fig. 9 shows schematically an “improved” fast RICH detector with pad read-out on the MWPC cathode. The presence of the GEM mesh between the main amplification element and the photo-cathode should also reduce the possibility and the dangerous effects of photon feedback.

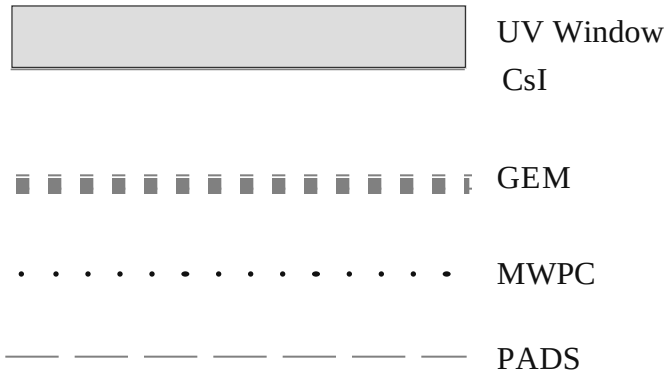

Fig. 9: Fast RICH detector with pre-amplification.

The GEM grid can easily be used as controlled gate to prevent ions feedback, or to select event similarly to the scheme used in pulse-gated Time Projection Chambers; the small value of the gating voltage would greatly reduce pick-up problems.

All described results have been obtained with a rather thin mesh (25 μm) resulting in a short multiplication path for electrons and therefore moderate gains. According to the authors of Refs. 4 and 5, in a parallel plate geometry the best results in terms of gain have been obtained for gaps close to 100 μm; if thicker GEM meshes provide similar results, one can envisage to replicate the MICROMEGAS and CAT high gain performances performances by simply laying a mesh over the stripped readout electrode; being cheap and self-supporting, this geometry should have definite advantages over the quoted designs.

Perhaps the most original use of GEM would be in a multi-stage gas electron multiplier, as shown in Fig. 10. Several composite grids, mounted within the same gas volume, and powered by a suitable resistor chain should allow to reach large gains, somewhat in analogy to multi-grid vacuum tubes, but substantially simpler and cheaper to manufacture for large areas; readout could be obtained with a terminal MWPC, MSGC or directly on a matrix of pads. The multiplier should operate in strong magnetic fields, with only some image distortions (Lorenz angle). For large gains, ions feedback and attachment to the insulator may become a problem, and should be studied.

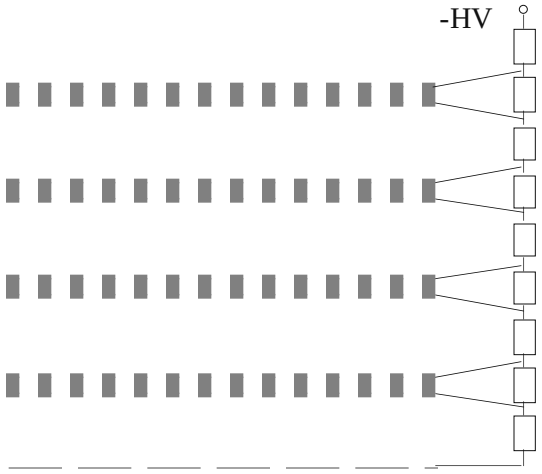

Fig. 10: A multi-grid GEM multiplier; read-out can be realized directly on strips or pads, or using a MWPC, MSGC or PPC.

As a final suggestion, one can think of developing non-planar GEM structures for special applications, cylindrical for tracking detectors around colliders and spherical for resolving the well know parallax error aberration in thick layer X-ray detectors such as those used for crystal diffraction studies

V. FURTHER DEVELOPMENTS

Much of the described applications and developments depend on the elaboration of a suitable, reliable technique to produce the GEM grids at low cost. Intrinsically simple and making use of well established printed circuit technologies, manufacturing of the multi-layer grids is nevertheless a delicate enterprise in view of the requirements (very good insulation between the two metals). Careful cleaning, not introducing any sort of conducting debris or stains, should be used, followed by proper conditioning; we have found that baking in vacuum at moderate temperature (~ 100 °C) improves the quality of the insulation. With CERN installations, good quality prints with 20 cm on the side can be manufactured today; larger sizes would require recourse to outside industry. Alternative methods for realizing the GEM structure are being investigated; a promising approach makes use of existing polymer high-precision meshes used as filters in the chemical industry and vacuum-coated on both sides with a thin layer of metal [2].

The influence of the insulator thickness on the maximum gain has to be investigated, as well as the possible charging up effects; if relevant, these effects could be controlled by the use of a moderate resistivity insulator, or with a thin resistive coating applied by non-directional deposition technologies such as Chemical Vapor Deposition in analogy of what is done to solve similar problems in MSGCs. Other industrial processes, such as those used to produce the low cost, large size micro-meshed used in the electronics industry should be investigated.

[2] G. Della Mea and V. Rigato, INFN Legnaro, Italy

VI. CONCLUSIONS AND SUMMARY

We have described a novel concept in gas amplification structures, a thin insulating mesh separating to two metal grids with a dense matrix of holes or channels, typically 50 μm in diameter. Inserted in the path of drifting electrons, the Gas Electron Multiplier allows to transfer the charge with an effective amplification; pre-amplification factors close to ten have been obtained with GEM grid implemented on a 25 μm thick insulator, but higher values can be expected with thicker layers (50 to 100 μm). The GEM grid is relatively easy to manufacture using standard multi-layer printed circuit technology, and large sizes can be envisaged. Inserted as pre-amplification element in various types of gas detectors, the GEM amplifier should allow to overcome some limitations intrinsic in the use of gaseous devices at high gains.

VII. REFERENCES

[1] F. Sauli,The Gas Electron Multiplier, submitted as Letter to Nucl. Instr. and Methods (1 Nov. 1996).

[2] G. Charpak and F. Sauli, Physics Letters 78B (1978) 523.

[3] M. Adams et al, Nucl. Instrum. Methods 217 (1983) 237.

[4] Y. Giomataris, Ph. Rebougeard, J.P. Robert and G. Charpak, Nucl. Instr. Meth. A376(1996)29.

[5] F.Bartol, M. Bordessoule, G. Chaplier, M. Lemonnier and S. Megtert, J. Phys.III 6(1996)337.

[6] R. Bouclier, M. Capeáns, G. Million, L. Ropelewski, F. Sauli, T. Temmel, R.A. Cooke, S. Donnel, S. Sastri and N. Sonderer, Nucl. Instrum. Methods A369 (1996) 328.

[7] R. Bouclier, M. Capeáns, C. Garabatos, G. Manzin, G. Million, L. Ropelewski, F. Sauli, T. Temmel, L. Shekhtman, V. Nagaslaev, Yu. Pestov and A. Kuleshov, Nucl. Instr. Meth. A365(1995)65.

[8] V. Peskov, B.D. Ramsey and P. Fonte, Int. Conf. on Position Sensitive Detectors (Manchester, 9-13 Sept. 1996).

[9] R. Bouclier, M. Capeáns, G. Manzin, L. Ropelewski, F. Sauli, A. Sharma, L. Shekhtman, CERN CMS TN/96-018.

[10] A. Breskin, Nucl. Instrum. Methods A371 (1996) 116.

The Gas Electron Multiplier (GEM)

R.Bouclier, M.Capeáns, W.Dominik, M.Hoch, J-C.Labbé, G.Million, L.Ropelewski, F.Sauli and A.Sharma[a]

CERN, CH-1211 Genève, Switzerland

[a] VUB-ULB Brussels, Belgium

Abstract

We describe operating principles and results obtained with a new detector element: the Gas Electrons Multiplier (GEM) [1]. Consisting of a thin composite sheet with two metal layers separated by a thin insulator, and pierced by a regular matrix of open channels, the GEM electrode, inserted on the path of electrons in a gas detector, allows to transfer the charge with an amplification factor approaching ten. Uniform response and high rate capability are demonstrated. Coupled to another device, multiwire or micro-strip chamber, the GEM electrode permits to obtain higher gains or less critical operation; separation of the sensitive (conversion) volume and the detection volume has other advantages: a built-in delay (useful for triggering purposes), and the possibility of applying high fields on the photo-cathode of ring imaging detectors to improve efficiency.

Multiple GEM grids in the same gas volume allow to obtain large amplification factors in a succession of steps, leading to the realization of an effective gas-filled photomultiplier.

I. INTRODUCTION

Methods for obtaining large, stable proportional gains in gaseous detectors are a continuing subject of investigation in the detector's community. Several years ago, Charpak and Sauli [2] introduced the Multi-Step Chamber (MSC) as a way to overcome some limitations of gain in Parallel Plate and Multi-Wire Proportional Chambers (MWPC); two parallel grid electrodes, mounted in the drift region of a conventional gas detector and operated as parallel plate multipliers, allow to pre-amplify drifting electrons and transfer them into the main detection element. Operated with a photo-sensitive gas mixture, the MSC allows to reach gains large enough for single photon detection in Ring Imaging Cherenkov (RICH) detectors [3].

More recently, Charpak and Giomataris have developed MICROMEGAS, a high gain gas detector using as multiplying element a narrow gap parallel plate avalanche chamber [4]. With gaps in the range 50 to 100 μm, realized by stretching a thin metal micro-mesh electrode parallel to a read-out plane, the authors

have demonstrated very high gain and rate capabilities, understood to result from the special properties of electron avalanches in very high electric fields.

The major practical inconvenience of both described detectors lies in the necessity of stretching and maintaining parallel meshes with very good accuracy; the presence of strong electrostatic attraction forces adds to the problem, particularly for large sizes. This requires heavy support frames, and in the case of MICROMEGAS, the introduction in the gap of closely spaced insulating lines or pins with the ensuing complication of assembly and loss of efficiency.

An interesting device recently developed, the CAT (*Compteur A Trou* [5]), consists of a matrix of holes drilled through a cathode foil; with the insertion of an insulating sheet between cathode and buried anodes, it allows to guarantee a good gap uniformity and to obtain high gains.

In the present paper, we describe a novel concept that seems to hold both the simplicity of the MSC scheme, and the high field advantages of MICROMEGAS and CAT, however mechanically much simpler to implement and more versatile: the Gas Electron Multiplier (GEM).

II. PRINCIPLE OF OPERATION

The basic element of the GEM detector is a thin, self-supporting three-layer mesh realized by the conventional photo-lithographic methods used to produce multi-layer printed circuits. A thin insulating polymer foil metallized on each side is passivated with photo-resist and exposed to light through a mask; after curing, the metal is patterned on both sides by wet etching and serves as self-alignment mask for the etching of the insulator in the open channels. We have obtained medium size meshes (5 by 5 cm^2) with 25 μm thick polymer sandwiched between 18 μm thick copper electrodes; the etching pattern has rows of 70 μm wide holes spaced 100 μm (Fig. 1); the fabrication technology, developed by the CERN Surface Treatment Service[1], can be extended to larger areas.

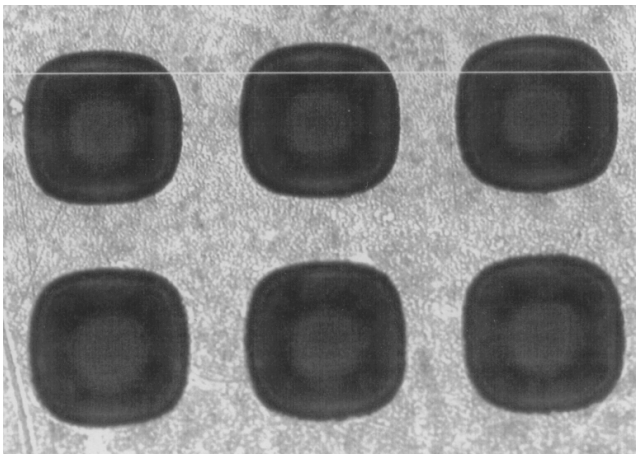

Fig. 1: Micro-photography of the three-layer (metal-insulator-metal) GEM grid. The distance betwen holes is 100 μm.

[1] R. De Oliveira, A. Gandi and L. Mastrostefano

Because of the etching process, holes are conical in shape from both entry sides, probably improving the dielectric rigidity (see Fig. 2). Upon application of a suitable difference of potential, the electric field in a channel of the GEM grid develops as shown in Fig. 2; for this calculation, the mesh has been inserted between two equidistant electrodes at symmetric potentials. From the data reported by the authors of Ref. 4, we expect to obtain multiplication in the high field in the center of the channel at a difference of potential around two hundred volts; for this value, the corresponding field strength along the central line is shown in Fig. 3: at the maximum, it reaches 40 kV cm^{-1}. Electrons produced by ionization in the upper gas volume drift into the channels, multiply in avalanche in the high field region and leave towards the electrodes in lower volume. Most of the ions generated in the avalanche recede along the central field lines, limiting the perturbing effects of the insulator charging up.

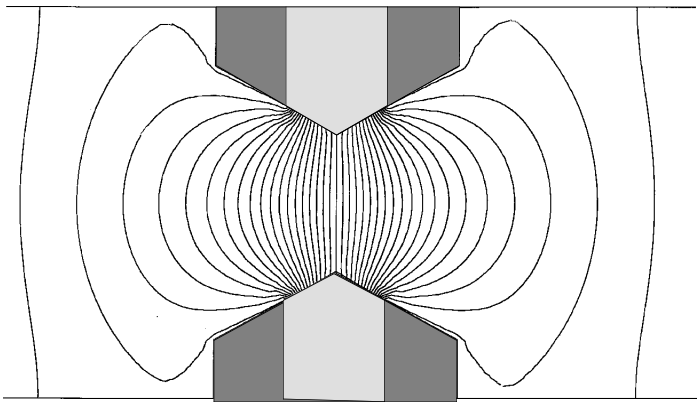

Fig. 2: Equipotentials lines in the GEM multiplying channel (V_{GEM} =200V).

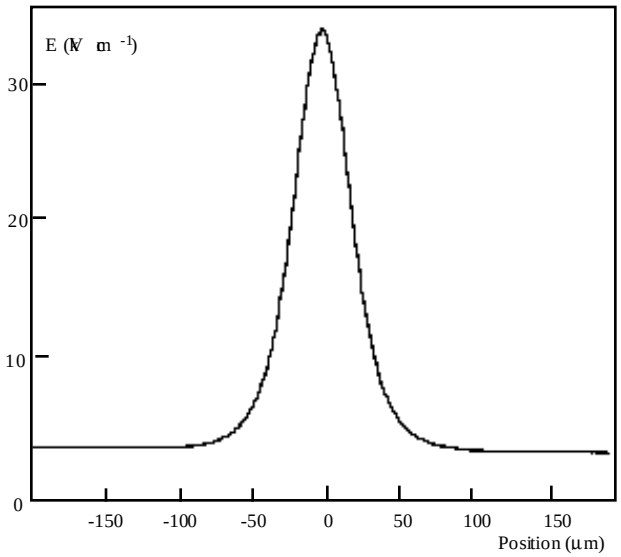

Fig. 3: Electric field along the central field line in the multiplying channel.

Thanks to the focusing effect of the field, one expects full efficiency for transfer of charge, and the dense channel spacing reduces image distortions. For the device to properly function, a good and regular insulation between the grid electrodes is required, with no sharp edges, metallic fragments or conducting deposits in the channel; this has been obtained by careful optimization of the etching and cleaning procedures. The first GEM mesh manufactured on our design had around a quarter million channels covering a square grid 50x50 mm^2, and was used for the measurements described in what follows. The test assembly is schematically shown in Fig. 4: a standard, small size MWPC is modified replacing one cathode with a thin printed circuit board holding the GEM mesh in the center; the mesh is pasted to the board, taking great care to avoid problems at the outer edge of the print (the metal on one side of the grid was removed for a few mm along the edges). Above the GEM electrode, a second cathode (the drift electrode) defines the sensitive volume of the detector.

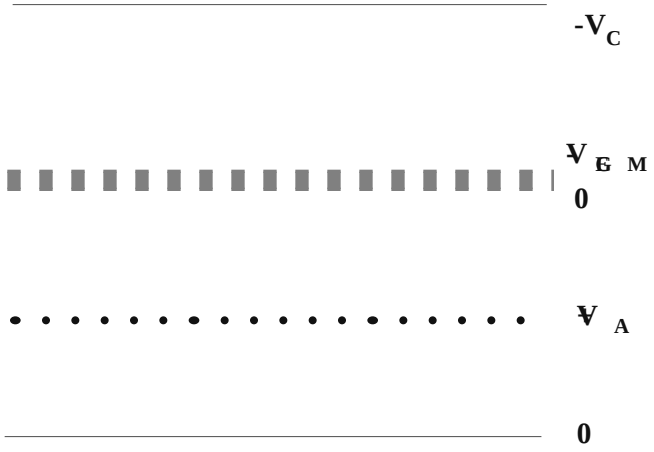

Fig. 4: Test assembly with the GEM multiplier mounted within a standard MWPC (drawing not to scale).

For convenience, the MWPC is operated with the anode wires at positive potentials, the signals being picking up through HV decoupling capacitors; this choice allows to maintain the lower electrode of GEM at ground potential, and easily increase the multiplying voltage. For ionization produced in the MWPC gaps, a regular process of collection and amplification takes place; electrons released in the upper drift region, on the contrary, can drift into and through the GEM channels and multiply, depending on potentials. Using a collimated X-ray source, one can easily disentangle the operation in the two regions. For most of this study, we have used a 5.9keV ^{55}Fe X-ray source; to measure the rate capability, the detector has been exposed to a collimated 8 keV beam from a generator.

III. EXPERIMENTAL RESULTS

A. Charge transfer and pre-amplification

In order to avoid having to reach excessive potentials across the GEM mesh, we have found convenient to operate the detector at low quencher levels; a good choice is a mixture of Argon and Dimethyl-ether (DME) in the proportion 90-10, used for all measurements described here. The detector operates however well in other mixtures, including some with the level of quencher below the flammability limit (3.5% for

DME). The MWPC is powered at a voltage providing a moderate gain (~10^4), keeping V_{GEM} grounded; the standard ^{55}Fe spectrum is recorded. With the upper drift electrode at fixed potential (typically -1 kV), the negative potential on GEM is progressively increased. At -V_{GEM}~50 V, a signal begins to appear, corresponding to charge transferred from the drift region; at ~140 V the transferred charge equals the direct one (100% transparency). Increasing -V_{GEM} further, the pre-amplified charge exceeds the direct component. Fig. 5 shows a typical pulse height spectrum, recorded at a pre-amplification factor around 6

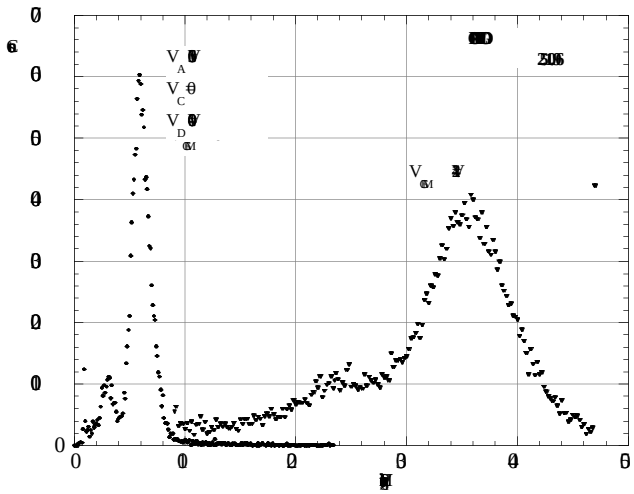

Fig. 5: ^{55}Fe pulse height spectrum recorded in the MWPC without (left) and with pre-amplification.

The energy resolution of the detector is not affected by the pre-amplification process; from Fig. 5 one can infer a resolution of around 11% r.m.s. for the pre-amplified charge, as compared to 12% r.m.s. for the direct signal (the apparent improvement is probably due to some non-linearity of the response)

Fig. 6 shows the measured pre-amplification factor, defined as the ratio of the most probable pulse height between transferred and direct spectra for the 5.9 keV line, as a function of the GEM voltage. In this particular mesh, the first to be realized, discharges appear at around -230 V; they are however without any consequence to the detector. From previous observations [6], we expect that use of a thicker insulator (50 to 100 μm instead of 25) could lead to higher effective gains.

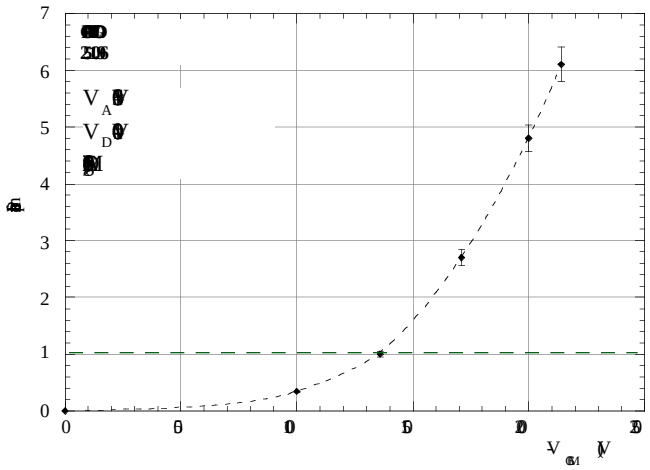

Fig. 6 Pre-amplification factor as a function of the difference of potential on the GEM grid.

The strength of the field in the drift region does not affect, in a wide range, the collection and transfer characteristics and the pre-amplification factor (although it affect other drift properties). We have seen no difference in transferred charge, at a pre-amplification factor around 6, varying the drift voltage from -500 to -2000 V. This can be exploited to tune drift velocity, diffusion and Lorentz angles according to experimental needs.

B

The uniformity of response of the detector has been measured by displacing the collimated source across the active area (50x50 mm^2); the gain is remarkably uniform (Fig. 7), with a maximum variation of ±4% (which includes the possible variations in the MWPC). Because of poor collimation of the source, the signal is detected on a slightly wider region than the opening of the grid.

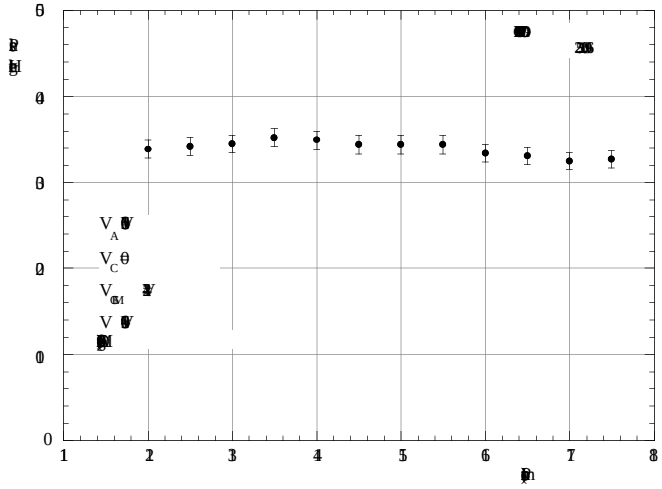

Fig. 7: Gain uniformity measured across the GEM grid.

C

To investigate possible gain reductions induced by charges deposited on the insulator surfaces within the channels, we have exposed the GEM detector to increasing rates of 8 keV X-rays from a generator. The irradiated area covered about 3 mm^2. It should be noted that the MWPC itself (with 2 mm wire spacing) is expected to suffer space charge gain drops at rates exceeding ~10^4 $mm^{-2}s^{-1}$. In order to be in similar conditions, the measurements were realized at constant total gain adjusting the MWPC anode potential. The preliminary results, Fig. 8, show no difference in behavior implying the absence of charging up processes in the GEM mesh.

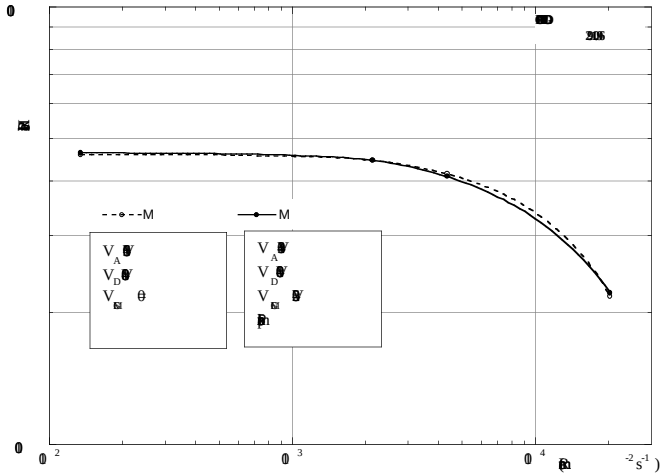

Fig. 8: Gain as a function of rate measured at equal gain for the MWPC and for the GEM+ MWPC chamber.

Coupled to a high-rate detector, such as the MSGC, the rate capability of GEM may be limited by charging-up of the insulator in the open channels. If such is the case, it can be envisaged either to use a moderate conductivity material for the layer (in the range 10^{10} to 10^{13} Ω.cm), or to coat the mesh by vacuum deposition or Chemical Vapor Deposition (CVD) with a thin controlled resistivity layer in the range 10^{14} to 10^{16} Ω, using technologies developed for MSGCs [7].

IV. APPLICATIONS

A variety of uses can be envisaged for the GEM mesh: self-supporting, the element can be easily incorporated in other structures. The added pre-amplification factor, even moderate, can ease the operation of any gain-critical detector.

In Micro-Strip Gas Chambers (MSGC) a serious problem of discharges has been met recently [8,9]. When operated close to their maximum gain limit in order to efficiently detect minimum ionizing particles, MSGCs can be irreversibly damaged by a discharge initiated by heavily ionizing tracks (recoils produced by neutrons, nuclear fragments); the effect is enhanced in presence of a high flux of radiation, and its probability depends strongly on the operating voltage [10]. The use of a GEM grid above the MSGC, with even a moderate pre-amplification, would allow to operate the MSGC well below the critical potential for

discharges. The moderate increase in the spatial extension of the detected charge, with its de-clustering effect, should also improve the localization accuracy; the added delay, corresponding to the drift time of electrons from GEM to the MSGC plate, could be exploited for the first level triggering.

A second application of the pre-amplification principle, already mentioned, could be in fast RICH detectors. Aside for allowing larger gain and therefore easing single photo-electron detection, the structure can be designed to exert a high electric field on the solid photo-cathode side of the detector, thus substantially improving its quantum efficiency [11]. Fig. 9shows schematically an "improved" fast RICH detector with pad read-out on the MWPC cathode. The presence of the GEM mesh between the main amplification element and the photo-cathode should also reduce the possibility and the dangerous effects of photon feedback.

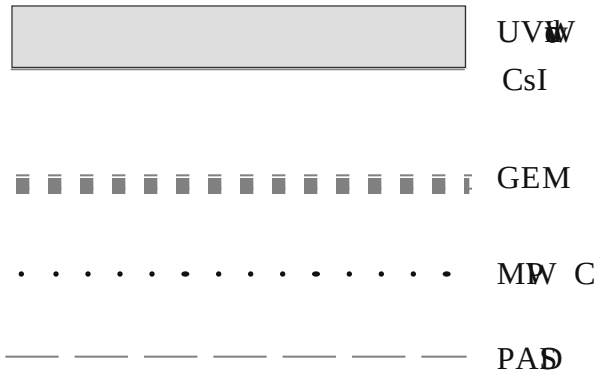

Fig. 9 Fast RICH detector with pre-amplification.

The GEM grid can easily be used as controlled gate to prevent ions feedback, or to select event similarly to the scheme used in pulse-gated Time Projection Chambers; the small value of the gating voltage would greatly reduce pick-up problems.

All described results have been obtained with a rather thin mesh (25 μm) resulting in a short multiplication path for electrons and therefore moderate gains. According to the authors of Refs. 4 and 5, in a parallel plate geometry the best results in terms of gain have been obtained for gaps close to 100 μm; if thicker GEM meshes provide similar results, one can envisage to replicate the MICROMEGAS and CAT high gain performances performances by simply laying a mesh over the stripped readout electrode; being cheap and self-supporting, this geometry should have definite advantages over the quoted designs.

Perhaps the most original use of GEM would be in a multi-stage gas electron multiplier, as shown in Fig. 10. Several composite grids, mounted within the same gas volume, and powered by a suitable resistor chain should allow to reach large gains, somewhat in analogy to multi-grid vacuum tubes, but substantially simpler and cheaper to manufacture for large areas; readout could be obtained with a terminal MWPC, MSGC or directly on a matrix of pads. The multiplier should operate in strong magnetic fields, with only some image distortions (Lorenz angle). For large gains, ions feedback and attachment to the insulator may become a problem, and should be studied.

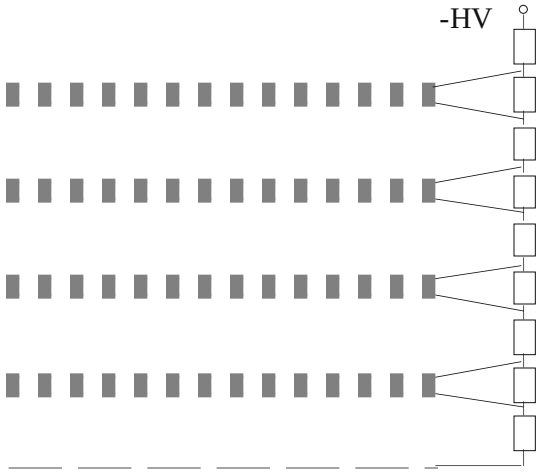

Fig. 10: A multi-grid GEM multiplier; read-out can be realized directly on strips or pads, or using a MWPC, MSGC or PPC.

As a final suggestion, one can think of developing non-planar GEM structures for special applications, cylindrical for tracking detectors around colliders and spherical for resolving the well know parallax error aberration in thick layer X-ray detectors such as those used for crystal diffraction studies

V. FURTHER DEVELOPMENTS

Much of the described applications and developments depend on the elaboration of a suitable, reliable technique to produce the GEM grids at low cost. Intrinsically simple and making use of well established printed circuit technologies, manufacturing of the multi-layer grids is nevertheless a delicate enterprise in view of the requirements (very good insulation between the two metals). Careful cleaning, not introducing any sort of conducting debris or stains, should be used, followed by proper conditioning; we have found that baking in vacuum at moderate temperature (~100 °C) improves the quality of the insulation. With CERN installations, good quality prints with 20 cm on the side can be manufactured today; larger sizes would require recourse to outside industry. Alternative methods for realizing the GEM structure are being investigated; a promising approach makes use of existing polymer high-precision meshes used as filters in the chemical industry and vacuum-coated on both sides with a thin layer of metal [2].

The influence of the insulator thickness on the maximum gain has to be investigated, as well as the possible charging up effects; if relevant, these effects could be controlled by the use of a moderate resistivity insulator, or with a thin resistive coating applied by non-directional deposition technologies such as Chemical Vapor Deposition in analogy of what is done to solve similar problems in MSGCs. Other industrial processes, such as those used to produce the low cost, large size micro-meshed used in the electronics industry should be investigated.

[2] G. Della Mea and V. Rigato, INFN Legnaro, Italy

V. CONCLUSIONS AND SUMMARY

We have described a novel concept in gas amplification structures, a thin insulating mesh separating to two metal grids with a dense matrix of holes or channels, typically 50 μm in diameter. Inserted in the path of drifting electrons, the Gas Electron Multiplier allows to transfer the charge with an effective amplification; pre-amplification factors close to ten have been obtained with GEM grid implemented on a 25 μm thick insulator, but higher values can be expected with thicker layers (50 to 100 μm). The GEM grid is relatively easy to manufacture using standard multi-layer printed circuit technology, and large sizes can be envisaged. Inserted as pre-amplification element in various types of gas detectors, the GEM amplifier should allow to overcome some limitations intrinsic in the use of gaseous devices at high gains.

VI. REFERENCES

[1] F. Sauli,The Gas Electron Multiplier, submitted as Letter to Nucl. Instr. and Methods (1 Nov. 1996).

[2] G. Charpak and F. Sauli, Physics Letters 78B (1978) 523.

[3] M. Adams et al, Nucl. Instrum. Methods 217 (1983) 237.

[4] Y.Giomataris, Ph. Rebougeard, J.P. Robert and G. Charpak, Nucl. Instr. Meth. A376(1996)29.

[5] F.Bartol, M. Bordessoule, G. Chaplier, M. Lemonnier and S. Megtert, J. Phys.III 6(1996)337.

[6] R. Bouclier, M. Capeáns, G. Million, L. Ropelewski, F. Sauli, T. Temmel, R.A. Cooke, S. Donnel, S. Sastri and N. Sonderer, Nucl. Instrum. Methods A369 (1996) 328.

[7] R. Bouclier, M. Capeáns, C. Garabatos, G. Manzin, G. Million, L. Ropelewski, F. Sauli, T. Temmel, L. Shekhtman, V. Nagaslaev, Yu. Pestov and A. Kuleshov, Nucl. Instr. Meth. A365(1995)65.

[8] V. Peskov, B.D. Ramsey and P. Fonte, Int. Conf. on Position Sensitive Detectors (Manchester, 9-13 Sept. 1996).

[9] R. Bouclier, M. Capeáns, G. Manzin, L. Ropelewski, F. Sauli, A. Sharma, L. Shekhtman, CERN CMS TN/ 96-018.

[10] A. Breskin, Nucl. Instrum. Methods A371 (1996) 116.